Title

Reduced Cognition in Syngap1 Mutants Is Caused by Isolated Damage within Developing Forebrain Excitatory Neurons

Journal

Neuron, 82(6)

ISSN

0896-6273

Authors

Ozkan, Emin D
Creson, Thomas K
Kramár, Enikö A
et al.

Publication Date

2014-06-01

DOI

10.1016/j.neuron.2014.05.015

Neuron
Article

Reduced Cognition in *Syngap1* Mutants Is Caused by Isolated Damage within Developing Forebrain Excitatory Neurons

Emin D. Ozkan,[1,5] Thomas K. Creson,[1,5] Enikö A. Kramár,[2] Camilo Rojas,[1] Ron R. Seese,[2] Alex H. Babyan,[2] Yulin Shi,[2] Rocco Lucero,[3] Xiangmin Xu,[2] Jeffrey L. Noebels,[3] Courtney A. Miller,[1,4] Gary Lynch,[2] and Gavin Rumbaugh[1,*]
[1]Department of Neuroscience, The Scripps Research Institute, Jupiter, FL 33458, USA
[2]Department of Anatomy and Neurobiology, University of California, Irvine, Irvine, CA 92797, USA
[3]Developmental Neurogenetics Laboratory, Departments of Neurology, Neuroscience, and Molecular and Human Genetics, Baylor College of Medicine, Houston, TX 77030, USA
[4]Department of Metabolism and Aging, The Scripps Research Institute, Jupiter, FL 33458, USA
[5]Co-first author
*Correspondence: grumbaug@scripps.edu
http://dx.doi.org/10.1016/j.neuron.2014.05.015

SUMMARY

Syngap1 **haploinsufficiency is a common cause of sporadic intellectual disability.** ***Syngap1*** **mutations disrupt developing pyramidal neurons, although it remains unclear if this process contributes to cognitive abnormalities. Here, we found that haploinsufficiency restricted to forebrain glutamatergic neurons was sufficient to disrupt cognition and removing mutations from this population prevented cognitive abnormalities. In contrast, manipulating** ***Syngap1*** **function in GABAergic neurons had no effect on cognition, excitability, or neurotransmission, highlighting the specificity of** ***Syngap1*** **mutations within forebrain excitatory neurons. Interestingly, cognitive abnormalities were reliably predicted by the emergence of enhanced excitatory synaptic function in mature superficial cortical pyramidal cells, which was a neurophysiological disruption caused by** ***Syngap1*** **dysfunction in developing, but not adult, forebrain neurons. We conclude that reduced cognition in** ***Syngap1*** **mutants is caused by isolated damage to developing forebrain glutamatergic neurons. This damage triggers secondary disruptions to synaptic homeostasis in mature cortical pyramidal cells, which perpetuates brain dysfunction into adulthood.**

INTRODUCTION

Intellectual disability (ID) is characterized by low IQ and behavioral deficits, reaching a prevalence of 1%–3% worldwide. This is a devastating brain disorder in which many patients are unable to care for themselves, placing a tremendous emotional and economic burden on families and society (Centers for Disease Control and Prevention, 2004; Doran et al., 2012). *SYNGAP1*/*Syngap1* (now referred to as *Syngap1* for simplicity) is among the most commonly mutated genes in sporadic ID. De novo autosomal dominant mutations in *Syngap1* that produce haploinsufficiency account for 2%–8% of these cases, and the majority of patients have more severe forms of ID (Berryer et al., 2013; de Ligt et al., 2012; Hamdan et al., 2009, 2011a, 2011b; Krepischi et al., 2010; Rauch et al., 2012). Considering the relatively high prevalence of sporadic ID in the population, the surprising frequency of pathogenic *Syngap1* mutations in enriched patient populations suggest that there are tens-of-thousands of undocumented individuals carrying these mutations. Affected individuals also have a high incidence of childhood seizures and autism spectrum disorder. *Syngap1* haploinsufficiency has been causally linked to epileptic encephalopathy, a devastating and often fatal form of childhood epilepsy that dramatically impairs cognitive development (Carvill et al., 2013). These recently identified patients with epileptic encephalopathy and *Syngap1* mutations also share ID and autism spectrum disorder comorbidities. Thus, proper *Syngap1* gene dosage is essential for the normal development of human cognition and appears to modify important aspects of neural excitability and sociability.

The *Syngap1* heterozygous knockout mouse line (*Syngap1*$^{+/-}$) has emerged as a robust model to understand the patho-neurobiology that underlies reduced cognitive ability and neural hyperexcitability in sporadic ID and epilepsy. *Syngap1*$^{+/-}$ mice display significant cognitive, emotional, and social abnormalities, which supports the idea that inactivating mutations of this gene directly cause cognitive impairment (Berryer et al., 2013; Guo et al., 2009; Komiyama et al., 2002; Muhia et al., 2010). Reduced *Syngap1* function in development accelerates the maturation of excitatory synaptic function in forebrain pyramidal cells (Clement et al., 2012, 2013), suggesting that damage to developing glutamatergic neurons may contribute to cognitive abnormalities in *Syngap1* mutants. However, a causal link between cognitive defects in *Syngap1* haploinsufficiency and developing glutamatergic neurons has not been shown. The change in glutamatergic neuron synapse development could be an inconsequential secondary outcome arising from dysfunction in other cell subtypes. Indeed, elegant studies in models of syndromic neurodevelopmental disorders (NDDs) have shown that a single pathogenic

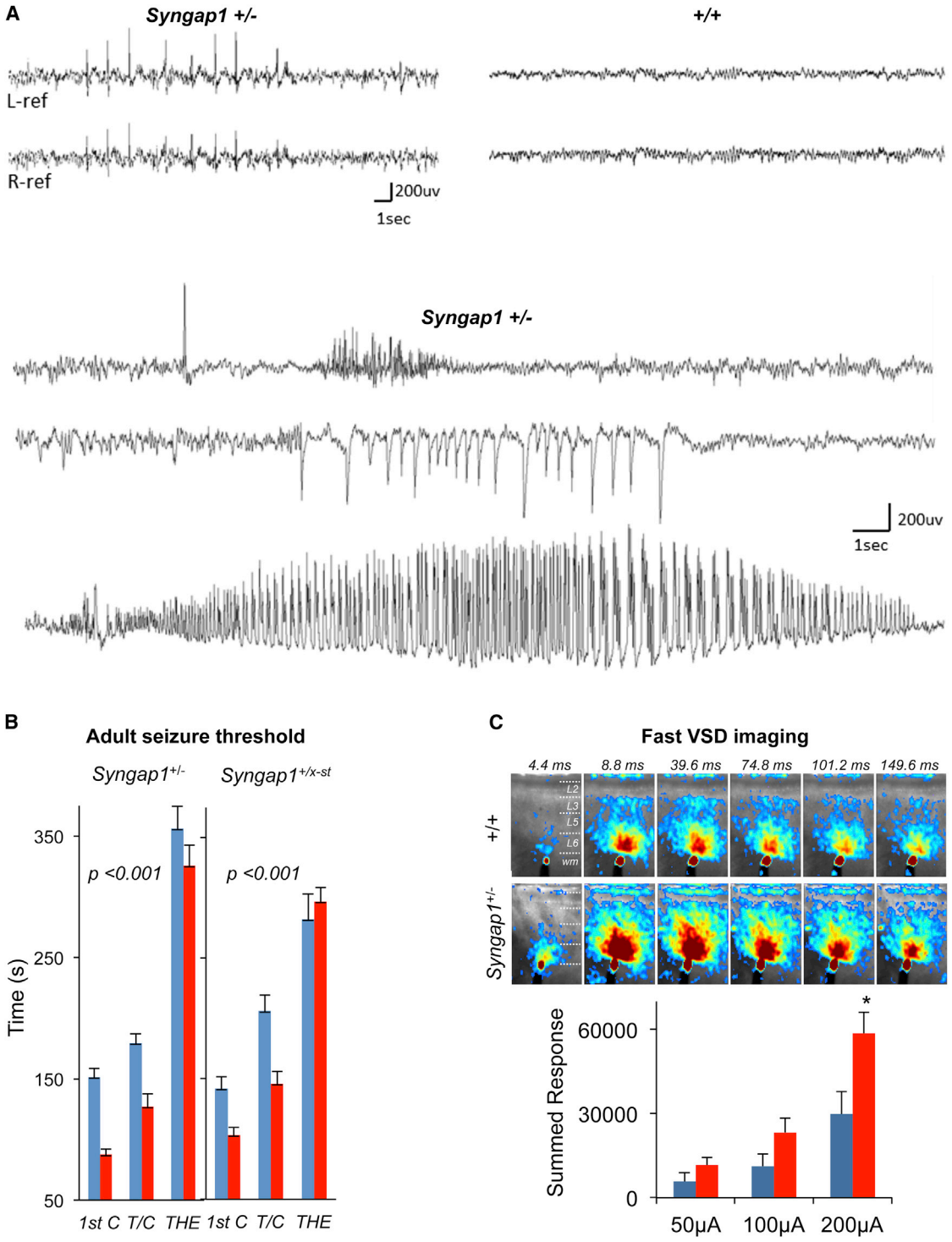

Figure 1. Altered EEG Activity, Reduced Seizure Threshold, and Cortical Hyperexcitability in Adult *Syngap1*$^{+/-}$ Mice

(A) Representative cortical EEG traces from chronically implanted, behaving Syngap1 +/− conventional mutant mice (n = 3) reveal frequent generalized sharp epileptiform discharges (upper left), and occasionally brief (<1 s) or prolonged (>10 s) seizures with a myoclonic jerk or little behavioral accompaniment during video monitoring (lower three traces). WT mice (n = 2) showed no evidence of hyperactive EEG spike discharges or seizures (top right). Electrodes record bilaterally from temporal and parietal cortices over left and right hemispheres in upper traces, and from left parietal cortex in lower seizure traces.

(B) Reduced flurothyl seizure threshold in both Syngap1+/− and Syngap1+/lx-st mutant mice (red bars) compared to WT controls (blue bars). Time (in seconds) taken to reach three separate events, first clonus (1st C), tonic-clonic (T/C), and total hindlimb extension (THE), during the course of the procedure were measured

(legend continued on next page)

mutation can affect the function of various cell types in the brain (Chao et al., 2010; Lioy et al., 2011). Furthermore, these studies demonstrate that multiple cell types are sufficient to drive cognitive, behavioral, and/or electrophysiological abnormalities in the CNS of NDD models. Thus, it remains unclear if altered development of glutamatergic neurons contributes importantly to cognitive deficits in *Syngap1* mutants. In addition, it is not known if other neuronal subtypes are also sufficient to drive cognitive abnormalities in these mice.

Complete restoration of *Syngap1* protein expression (SynGAP) in adult mutants has no detectable benefit on behavior and cognition, demonstrating that *Syngap1* haploinsufficiency is a disorder of brain development (Clement et al., 2012). Interestingly, all currently reported baseline neurophysiological abnormalities observed in young glutamatergic neurons of *Syngap1*$^{+/-}$ mice, such as enhanced excitatory synaptic transmission, are transiently expressed during development (Clement et al., 2012, 2013). Thus, it also remains unclear how *Syngap1* mutations in development affect adult brain function. Indeed, because the abnormal cognition persists throughout life, these findings suggest that there are undiscovered neurophysiological abnormalities in adult mice that arise from abnormal brain development and reflect abnormal cognition. To explore causal links between *Syngap1* dysfunction in developing glutamatergic neurons, stabilized changes to adult brain function, and altered cognitive ability, we combined cell-type specific and inducible conditional mouse lines with behavioral endophenotyping and electrophysiology. Using this approach, we found that germline *Syngap1* mutations induced a persistent form of stabilized cortical hyperexcitability that lasted into adulthood. Remarkably, this was caused exclusively by abnormal function of developing glutamatergic neurons located in the forebrain, because no phenotypic role for *Syngap1* in neurons that release GABA was apparent. Unexpectedly, abnormalities in developing glutamatergic neurons caused an emergent, secondary disruption to glutamatergic synaptic strength in adult neurons that reliably predicted the presence of reduced cognition. These data demonstrate that altered neurodevelopmental processes in a single sensitive cell type can perpetuate brain dysfunction into adulthood by altering excitatory/inhibitory (E/I) balance through a disruption of synaptic homeostasis.

RESULTS

Cortical Hyperexcitability and Progressively Worsening Superficial Pyramidal Cell E/I Balance in Adult Syngap1 Mutants

We sought to investigate how altered brain development in *Syngap1*$^{+/-}$ mice disrupts the function of the adult CNS. First, we performed electroencephalography (EEG) paired with video monitoring to examine spontaneous cortical activity in mutants (Figure 1A), which revealed frequent and widespread cortical discharges of high amplitude in mature *Syngap1*$^{+/-}$ mice (>12 weeks), but not in wild-type (WT) littermates. These epileptiform discharges were intermittent, ranging in frequency from 1 to 681/hour (average 81/hr). However, they did not coincide with any significant motor events. Interestingly, cortical generalized seizures with myoclonic features have also been reported in patients with *Syngap1* loss of function mutations (Berryer et al., 2013) and with lower cognitive ability (Carvill et al., 2013). We reasoned that cortical hyperexcitability might reflect a reduced seizure threshold in adult mutants. A flurothyl-induced activation paradigm (Clement et al., 2012) revealed a clear reduction in seizure threshold in two distinct *Syngap1* haploinsufficient mouse lines (Figure 1B). To determine if network hyperexcitability in mutants was preserved in ex vivo preparations, we performed fast voltage-sensitive dye (VSD) imaging in acute brain slices derived from adult *Syngap1* animals. Slices from adult *Syngap1*$^{+/-}$ mice resulted in significantly larger signals throughout the cortex when compared to slices derived from WT littermates (Figure 1C).

Because SynGAP is a potent regulator of glutamatergic synapse function (Clement et al., 2012, 2013; Rumbaugh et al., 2006), we hypothesized that elevated unitary synaptic strength in cortical pyramidal neurons contributes to slice hyperexcitability. To test this idea, we measured miniature excitatory postsynaptic currents (mEPSCs) from medial prefrontal cortex (mPFC) layer 2/3 (L2/3) neurons in acute slices prepared from WT or *Syngap1*$^{+/-}$ mice (Figures 2A and 2B). Interestingly, mEPSCs were normal in young cortical neurons (Figures 2C–2E). However, by adulthood, there was an increase in both the amplitude and frequency of the events (Figures 2F–2H). We also patched neurons in slices derived from the *Syngap1*$^{+/lx\text{-}st}$ mice. Neurons from this mouse line also exhibited enhanced mEPSC function in Layer 2/3 neurons (Figures 2I–K). To determine if the E/I ratio was disrupted in L2/3 pyramidal neurons, we acquired miniature inhibitory postsynaptic currents (mIPSCs) from neurons in slices derived from adult *Syngap1*$^{+/-}$ or WT littermates. There was a reduction in mIPSC amplitude in conventional *Syngap1*$^{+/-}$ mice (Figure 2L), but no change in mIPSC properties in the *Syngap1*$^{+/lx\text{-}st}$ mice (Figure 2M). However, because excitatory unitary synaptic strength was increased in both models relative to GABAergic neuron synaptic transmission, this is consistent with an elevated E/I ratio in mature mPFC cortical neurons in mice with *Syngap1* haploinsufficiency. Furthermore, L2/3 neurons were hyperexcitable in response to evoked neurotransmitter release (Figure S1 available online). We next measured

and plotted in the y axis. *Syngap1*$^{+/-}$: RMANOVA; genotype effect, F(1,19) = 20.46, p = 0.00023; genotype x event interaction, F(2, 38) = 0.99, p = 0.38. *Syngap1*$^{+/lx\text{-}st}$: RMANOVA; genotype effect, F(1,24) = 5.47,p = 0.028; genotype x event interaction, F(2,48) = 6.46, p = 0.0033.

(C) *Syngap1*$^{+/-}$ mPFC slices exhibit higher evoked excitability compared to WT control slices when examined with fast VSD imaging. (Top) Example time series data from VSD imaging of evoked circuit activity in response to electrical stimulation of 200 μA at 1 ms. All image frames were averaged over eight separate trials. The color scale codes VSD signal amplitude expressed as SD multiples above the mean baseline. Warmer colors indicate greater excitation. (Bottom) Pixel-based response analysis (see Experimental Procedures). The y axis shows the summed response (in the SD multiple units) across the defined response frames to electrical stimulation. Student's t test: 50 μA, n = 7 WT, n = 7 mutant, t(12) = 1.44, p = 0.18; 100 μA, n = 8 WT, n = 8 mutant, t(14) = 1.78, p = 0.096; 200 μA, n = 8 WT, n = 7 mutant, t(13) = 2.59, p = 0.022.

WT (+/+), blue; mutants (+/−), red for all bar graphs. Error bars represent SEM. *p < 0.05.

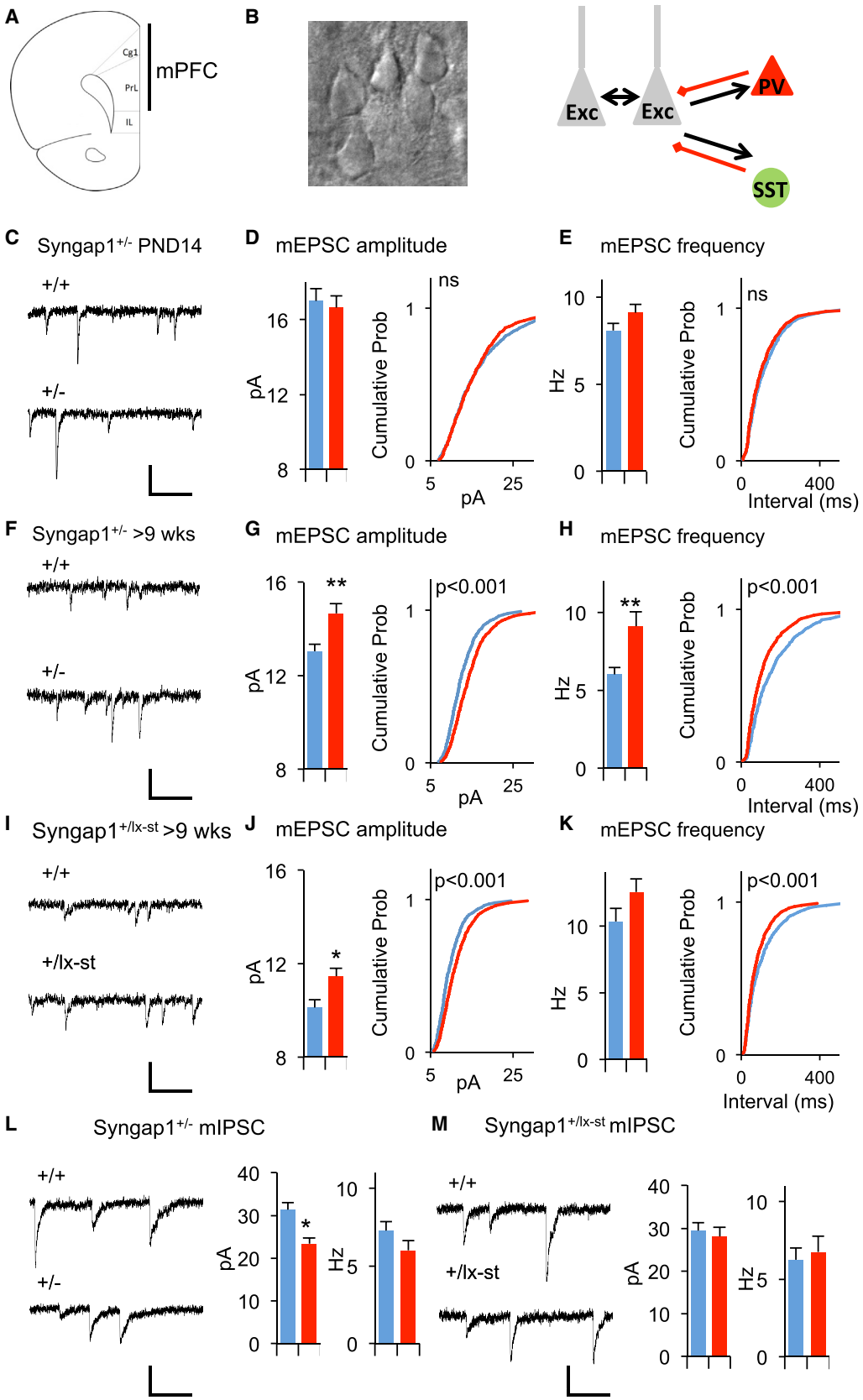

(legend on next page)

electrically isolated excitatory and inhibitory evoked responses from individual L2/3 pyramidal cells in mPFC slices from adult WT and *Syngap1* mutants (Figures S1A–S1C). There was no significant effect of peak excitatory responses in the basal pathway, although there was an increase in the slope of the input/output curve (Figures S1D and S1E). Importantly, evoked E/I balance was significantly shifted in both pathways (Figures S1L and S1M), which is consistent with our mEPSC/mIPSC data and supports the conclusion that L2/3 neurons are hyperexcitable in *Syngap1* mutants.

To this point, our measurements have been restricted to synaptic properties of L2/3 pyramidal neurons. However, there are other possible cellular causes of network hyperexcitability, such as alterations to the function of distinct classes of local inhibitory neurons in the superficial cortex (Figure 2B). Therefore, we probed Syngap1 mutants for changes in two major subtypes of cortical GABAergic neurons. To label Parvalbumin-positive (PV+) neurons in the *Syngap1*$^{+/-}$ background, we crossed *Syngap1*$^{+/-}$ mice that also contained the Ai9 Cre-dependent reporter allele (Madisen et al., 2010) with PV+-*ires*-Cre driver mice (Hippenmeyer et al., 2005; Figure 3A). tdTomato+ (TD+) neurons from both genotypes exhibited properties consistent with those of PV+ neurons (Table S1; Helm et al., 2013; Lazarus and Huang, 2011). There were no genotype differences in firing properties of these cells at PND 14 (Figure 3B). In contrast, there was a substantial decrease in firing rate in PV+ neurons in *Syngap1*$^{+/-}$ mice by 6 weeks of age (Figure 3C), which was consistent with cortical hyperexcitability. Interestingly, by 9 weeks of age, the difference between genotypes was no longer significant (Figure 3D). We next measured unitary synaptic strength onto PV+ neurons in mature animals. Overall, there was a small reduction in mEPSC amplitude in PV+ neurons (Figure 3E). However, this was only present in males (two-way ANOVA for PV+ mEPSC amplitude: genotype effect, $F_{(1,61)} = 6.00$, $p = 0.02$; sex effect $F_{(1,61)} = 5.01$, $p = 0.03$; genotype*sex $F_{(1,61)} = 4.72$, $p = 0.03$). In contrast, there was no sex-genotype interaction in L2/3 pyramidal cell mEPSC properties (two-way ANOVA for L2/3 neuron mEPSC amplitude: genotype effect, $F_{(1,102)} = 11.22$, $p = 0.0011$; sex effect, $F_{(1,102)} = 6.24$, $p = 0.014$;genotype*sex, $F_{(1,102)} = 0.054$, $p = 0.81$. Two-way ANOVA for L2/3 neuron mEPSC frequency: genotype effect, $F_{(1,102)} = 17.42$, $p = 0.0000629$; sex effect, $F_{(1,102)} = 0.003$, $p = 0.96$;genotype*sex, $F_{(1,102)} = 0.35$, $p = 0.55$; combined data). Thus, PV+ neurons may contribute to hyperexcitability at some stages of development, but individual changes in cellular and synaptic properties in these neurons do not stabilize in the fully mature CNS. We next probed for potential cellular disruptions in somatostatin-positive (SST+) local inhibitory neurons. Surprisingly, there were no genotype effects in any major cellular or synaptic measures in adult (>9 weeks) SST+ neurons (Figures 3F–3I; Table S1). There was a robust increase in action potential width of these neurons. However, this is a relatively minor physiological disruption with an unknown impact on network function (Table S1). Together, these data indicate that critical measures of inhibition are largely unaffected in the fully mature superficial cortex of *Syngap1* mutants.

E/I Imbalance Predicts Cognitive Abnormalities and Results from Syngap1 Dysfunction Exclusively in Glutamatergic Neurons of the Developing, but Not Mature, Forebrain

Increased pyramidal cell excitatory synaptic strength appeared to be a reliable signature of altered neurophysiological function in the mutant cortex, suggesting that *Syngap1* haploinsufficiency is principally a disease of altered glutamatergic neuron function. However, an abundance of SynGAP protein is found in both glutamatergic and GABAergic neurons in various cortical and subcortical areas of the brain, including heavy expression in the striatum (Moon et al., 2008; Porter et al., 2005; Zhang et al., 1999). Therefore, we explored the behavioral contribution

Figure 2. The Gradual Development of E/I Imbalance in L2/3 Pyramidal Neurons in *Syngap1*$^{+/-}$ Mice

(A) A coronal section through the mouse brain illustrating where in the mPFC targeted whole-cell recordings were performed. Cg1, cingulated cortex area 1; PL, prelimbic cortex; IL, infralimbic cortex.

(B) A high-magnification differential interference contrast image of example L2/3 neurons and simplified diagram of L2/3 circuitry.

(C) Example recordings of mEPSC events in PND14 *Syngap1*$^{+/-}$ animals. Scale bar represents 20 pA, 100 ms.

(D) Bar graph and cumulative percentage plots show normal mEPSC amplitude in PND14 *Syngap1*$^{+/-}$ animals (n = 15 neurons +/+, n = 14 neurons +/−; $t(27) = 0.40$, $p = 0.69$; two sample K-S test on cumulative percentage distribution $Z = 1.17$, $p = 0.13$).

(E) Bar graph and cumulative percentage plots show normal mEPSC frequency in PND14 *Syngap1*$^{+/-}$ animals (n = 15 neurons +/+, n = 14 neurons +/−; $t(27) = 1.66$, $p = 0.11$; two sample K-S test on cumulative percentage distribution $Z = 1.14$, $p = 0.15$).

(F) Example recordings of mEPSC events in >9-week-old *Syngap1*$^{+/-}$ animals. Scale bar represents 20 pA, 100 ms.

(G) Bar graph and cumulative percentage plots show increased mEPSC amplitude in >9-week-old *Syngap1*$^{+/-}$ animals (n = 12 neurons +/+, n = 11 neurons +/−; $t(21) = 3.61$, $p = 0.0016$; two sample K-S test on cumulative percentage distribution $Z = 4.34$, $p < 0.001$).

(H) Bar graph and cumulative percentage plots show increased mEPSC frequency in >9-week-old *Syngap1*$^{+/-}$ animals (n = 12 neurons +/+, n = 11 neurons +/−; $t(21) = 3.02$, $p = 0.0065$; two sample K-S test on cumulative percentage distribution $Z = 3.99$, $p < 0.001$).

(I) Example recordings of mEPSC events in >9-week-old *Syngap1*$^{+/lx\text{-}st}$ animals. Scale bar represents 20 pA, 100 ms.

(J) Bar graph and cumulative percentage plots show increased mEPSC amplitude in >9-week-old +/lx-st animals (n = 9 neurons +/+, n = 14 neurons +/−; $t(21) = 2.57$, $p = 0.018$; two sample K-S test on cumulative percentage distribution $Z = 5.42$, $p < 0.001$).

(K) Bar graph and cumulative percentage plots show slightly increased mEPSC frequency in >9-week-old +/lx-st animals (n = 9 neurons +/+, n = 14 neurons +/−; $t(21) = 1.50$,$p = 0.15$; two sample K-S test on cumulative percentage distribution $Z = 3.53$, $p < 0.001$).

(L) Bar graphs and example recordings show reduced mIPSC amplitude and normal mIPSC frequency in >9-week-old *Syngap1*$^{+/-}$ animals. (n = 12 neurons +/+, n = 12 neurons +/−; $t(22) = 2.57$, $p = 0.02$ for mIPSC amplitude; $t(22) = 0.88$, $p = 0.39$ for mIPSC frequency). Scale bar represents 30 pA, 100 ms.

(M) Bar graphs and example recordings show normal mIPSC amplitude and normal mIPSC frequency in >9-week-old *Syngap1*$^{+/lx\text{-}st}$ animals. (n = 9 neurons +/+, n = 7 neurons +/−; $t(14) = 0.48$, $p = 0.64$ for mIPSC amplitude; $t(14) = 0.40$, $p = 0.70$ for mIPSC frequency). Scale bar represents 20 pA, 100 ms.

WT(+/+), blue; mutants(+/−), red for all bar graphs. Error bars represent SEM. *$p < 0.05$, **$p < 0.01$.

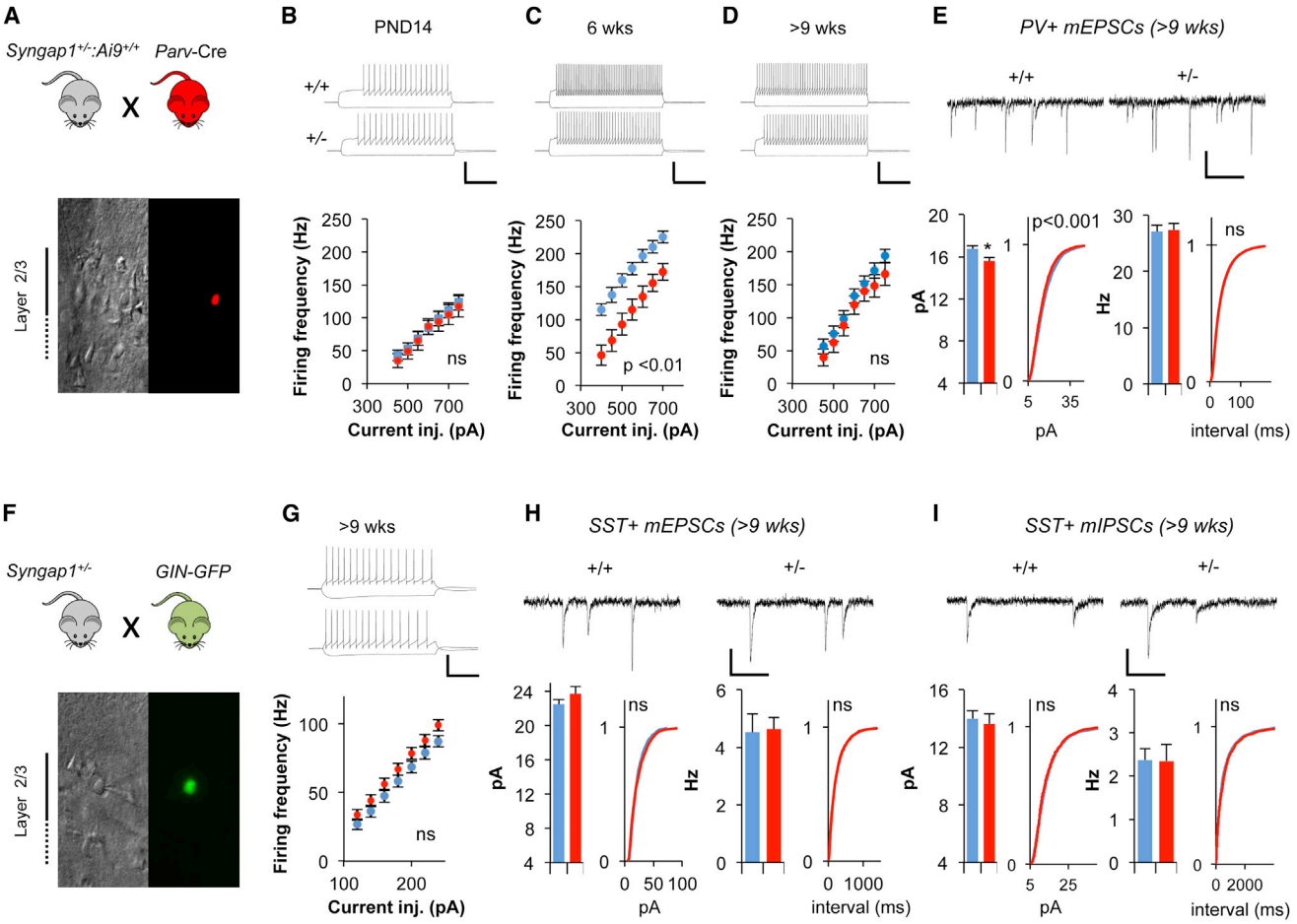

Figure 3. Intrinsic and Synaptic Properties of L2/3 Inhibitory Neurons in *Syngap1*$^{+/-}$ Mice

(A) Experimental strategy to record from PV+ interneurons in L2/3. Images show differential interference contrast and fluorescent image of a PV+ interneuron.

(B) Normal current injection frequency response curve of PV+ interneurons at PND14. Example traces show firing responses of +/+ and +/− neurons in response to 450 pA, 1 s long current injection (n = 11 neurons +/+, n = 11 neurons +/−, repeated-measures ANOVA genotype effect F(1,20) = 0.11,p = 0.75, genotype*stimulus level F(6,120) = 0.11, p = 0.99). Scale bar represents 50 mV, 300 ms.

(C) Reduced current injection frequency response curve of PV+ interneurons at 6 weeks. Example traces show firing responses of +/+ and +/− neurons in response to 450 pA, 1 s long current injection (n = 15 neurons +/+, n = 16 neurons +/−, repeated-measures ANOVA genotype effect F(1,29) = 14.74, p = 0.001 genotype*stimulus level F(6,174) = 1.67, p = 0.13). Scale bar represents 50 mV, 300 ms.

(D) Normal current injection frequency response curve of PV+ interneurons at >9 weeks. Example traces show firing responses of +/+ and +/− neurons in response to 450 pA, 1 s long current injection (n = 18 neurons +/+, n = 18 neurons +/−, repeated-measures ANOVA genotype effect F(1,34) = 0.87, p = 0.36, genotype*stimulus level F(6,204) = 0.864, p = 0.52). Scale bar represents 50 mV, 300 ms.

(E) Reduced excitatory input into PV+ interneurons. (Top) Example recordings of mEPSC events in PV+ interneurons. (Left) Bar graph and cumulative percentage plots show reduced mEPSC amplitude in PV+ interneurons (n = 31 neurons +/+, n = 34 neurons +/−; t(63) = 2.63, p = 0.01; two sample K-S test on cumulative percentage distribution Z = 2.15, p = 0.0002). (Right) Bar graph and cumulative percentage plots show normal mEPSC frequency in PV+ interneurons (n = 31 neurons +/+, n = 34 neurons +/−; t(63) = 0.14, p = 0.88; two sample K-S test on cumulative percentage distribution; Z = 0.58, p = 0.89). Scale bar represents 15 pA, 125 ms.

(F) Experimental strategy to record from somatostatin-positive (SST+) interneurons in L2/3. Pictures show differential interference contrast and fluorescent image of a SST+ interneuron.

(G) Normal current injection frequency response curve of SST+ interneurons at >9 weeks. Example traces show firing responses of +/+ and +/− neurons in response to 120 pA, 1 s long current injection (n = 23 neurons +/+, n = 21 neurons +/−, repeated-measures ANOVA genotype effect F(1,42) = 1.77, p = 0.19, genotype*stimulus level F(6,252) = 1.02, p = 0.41). Scale bar represents 50 mV, 300 ms.

(H) Normal excitatory input into SST+ interneurons. (Top) Example recordings of mEPSC events in SST+ interneurons. (Left) Bar graph and cumulative percentage plots show normal mEPSC amplitude in SST+ interneurons (n = 12 neurons +/+, n = 15 neurons +/−; t(25) = 1.19, p = 0.24; two sample K-S test on cumulative percentage distribution Z = 1.25, p = 0.087). (Right) Bar graph and cumulative percentage plots show normal mEPSC frequency in SST+ interneurons (n = 12 neurons +/+, n = 15 neurons +/−; t(25) = 0.15, p = 0.88; two sample K-S test on cumulative percentage distribution Z = 0.77, p = 0.59). Scale bar represents 15 pA, 125 ms.

(I) Normal inhibitory input into SST+ interneurons. (Top) Example recordings of mIPSC events in SST+ interneurons. (Left) Bar graph and cumulative percentage plots show normal mIPSC amplitude in SST+ interneurons (n = 34 neurons +/+, n = 22 neurons +/−; t(54) = 0.38, p = 0.71; two sample K-S test on cumulative

(legend continued on next page)

of in vivo *Syngap1* dysfunction in distinct cellular populations. In the first set of experiments, we crossed the conditional knockout line (*Syngap1*$^{+/fl}$; Clement et al., 2012) with EMX1-ires-Cre driver mice (Gorski et al., 2002). This mouse driver line induces Cre-mediated recombination in forebrain glutamatergic neurons and glia (Figure 4A). Importantly, SynGAP is a neuron-enriched gene (Chen et al., 1998; Kim et al., 1998; Kozlenkov et al., 2014) with no observable expression in glial cells (G.R., unpublished data), indicating that this Cre driver line is an excellent tool to determine if *Syngap1* genetic damage in developing cortical pyramidal cells is sufficient to disrupt cognitive development. SynGAP levels were reduced in the hippocampus, but not striatum, in extracts taken from Emx1-Cre;*Syngap1*$^{+/fl}$ mice (Figure 4B). Importantly, a reduction in SynGAP protein levels was also observed in the frontal cortex (Figure S2). The behaviors displayed by Emx1-Cre;*Syngap1*$^{+/fl}$ mice were indistinguishable from those of conventional *Syngap1* mutants. Relative to WT littermates, EMX1-Cre;*Syngap1*$^{+/fl}$ mice spent more time in the open arm of the elevated plus maze (Figure 4C), were hyperactive in the open field (Figure 4D), and failed to spontaneously alternate (Figure 4E). Conventional *Syngap1* Het mice had deficits in remote (30 day old) fear memory (Figure S3), allowing us to include an additional measure of cognition in the behavioral battery. Again, similar to conventional Syngap1 mutants, Emx1-Cre;*Syngap1*$^{+/fl}$ mice exhibited a remote memory deficit (Figure 4F). We next assessed adult seizure threshold. Consistent with the behavioral endophenotyping results, the Emx1-Cre;*Syngap1*$^{+/fl}$ mice also had a reduced seizure threshold (Figure 4G) that was qualitatively similar to conventional germline *Syngap1* mutants (Figure 1B).

To induce haploinsufficiency in developing GABAergic neurons, we next crossed *Syngap1* conditional knockout mice to Gad2-*ires*-Cre driver mice (Taniguchi et al., 2011; Figure 4H). A reduction in SynGAP expression in the striatum, but not hippocampus, confirmed haploinsufficiency in the target neuronal population (Figure 4I). Unexpectedly, SynGAP levels in the hippocampus of Gad2-Cre mice increased slightly. Therefore, we also probed SynGAP expression levels in the frontal cortex of Gad2-Cre;*Syngap1*$^{+/fl}$ mice. There was no change in SynGAP expression (Figure S2), which is consistent with low expression of SynGAP in cortical GABAergic neurons (Zhang et al., 1999). Surprisingly, despite SynGAP expression being reduced in GABAergic neurons in the CNS, including the striatum, there were no changes in behavior or seizure threshold (Figures 4J–4N).

If disruptions to forebrain glutamatergic neurons are the primary driver of the endophenotype in *Syngap1*$^{+/-}$ mice, then rescuing the mutation exclusively in this population should protect animals from developing behavioral abnormalities. To test this, we crossed EMX1- or GAD2-ires-Cre driver mice to the *Syngap1* conditional rescue line (*Syngap1*$^{+/lx\text{-}st}$; Clement et al., 2012; Figures 5A and 5G). Remarkably, reversing the pathogenic mutations only in forebrain glutamatergic neurons (Emx1-Cre;*Syngap1*$^{+/lx\text{-}st}$ mice) was sufficient to protect animals from developing major behavioral impairments, including altered anxiety and risk-taking, reduced working memory, and disrupted remote contextual memory (Figures 5B–5F). Interestingly, Emx1-Cre;*Syngap1*$^{+/lx\text{-}st}$ mice were still hyperactive in the open field (Figure 5C) and exhibited a reduced seizure threshold (Figure 5F), suggesting that extracortical neurons contribute to these abnormalities. This notion was supported by the observation that seizure threshold was rescued after global reversal of *Syngap1* haploinsufficiency (Figure S4). In a complementary set of experiments, reversal of a pathogenic *Syngap1* mutation in GABAergic neurons located throughout the entire CNS (Gad2-Cre;*Syngap1*$^{+/lx\text{-}st}$) provided no improvement to core *Syngap1* behavioral abnormalities (Figure 5H–5L).

Enhanced excitatory synaptic function in mature pyramidal neurons is present in both of our models of *Syngap1* haploinsufficiency (Figures 2F–2K). These data suggested that this neurophysiological abnormality is predictive of cognitive dysfunction and/or hyperexcitability in *Syngap1* mutants. To test this, we patch-clamped L2/3 neurons in mPFC acute slices taken from EMX1- and Gad2-ires-Cre mice crossed to each of our conditional *Syngap1* mutant lines. Both Emx1-Cre;*Syngap1*$^{+/fl}$ (forebrain glutamatergic conditional disruption) and Gad2-Cre;*Syngap1*$^{+/lx\text{-}st}$ (GABAergic neuron rescue) animals, which were offspring that had reduced cognition and altered seizure thresholds (Figures 4C–4G and 5G–5L), had enhanced excitatory synaptic strength in L2/3 mPFC pyramidal neurons (Figures 6A–6C, 6J, and 6K). Interestingly, no changes to pyramidal cell synaptic function were observed in either Gad2-Cre;*Syngap1*$^{+/fl}$ (GABAergic conditional disruption) or Emx1-Cre;*Syngap1*$^{+/lx\text{-}st}$ (forebrain glutamatergic neuron rescue) lines (Figures 6D–6I), which were offspring that had normal cognitive ability. We also tested the reliability of the reduced mIPSCs observed in *Syngap1*$^{+/-}$ line as a signature of cognitive ability, but found that neither Emx1-Cre;*Syngap1*$^{+/fl}$ nor Gad2-Cre;*Syngap1*$^{+/fl}$ displayed reduced mIPSCs (Figure S5). These data indicate that excitatory synaptic function in mature superficial pyramidal neurons reliably predicts cognitive ability, but not behavioral seizure threshold, in adult *Syngap1* mutant mice.

In the next set of experiments, we further explored the relationship between enhanced excitatory synaptic strength in L2/3 pyramidal neurons and cognitive disability in *Syngap1* mutants. To do this, we induced global *Syngap1* haploinsufficiency in mature animals and then probed for physiological and behavioral changes (Figure 7A). We first confirmed that tamoxifen injections reduced SynGAP protein by 50% in the experimental animals (Figure 7B), which is the level of expression observed in germline heterozygous knockout mice (Clement et al., 2012). Despite the conditional reduction of SynGAP protein in adulthood, mEPSC amplitude or frequency were not changed (Figures 7C and 7D),

percentage distribution Z = 1.15, p = 0.14). (Right) Bar graph and cumulative percentage plots show normal mIPSC frequency in SST+ interneurons (n = 34 neurons +/+, n = 22 neurons +/−; t(54) = 0.15, p = 0.88; two sample K-S test on cumulative percentage distribution Z = 1.26, p = 0.084). Scale bar represents 15 pA, 125 ms.

WT(+/+), blue; mutants(+/−), red for all bar graphs. Error bars represent SEM. *p < 0.05.

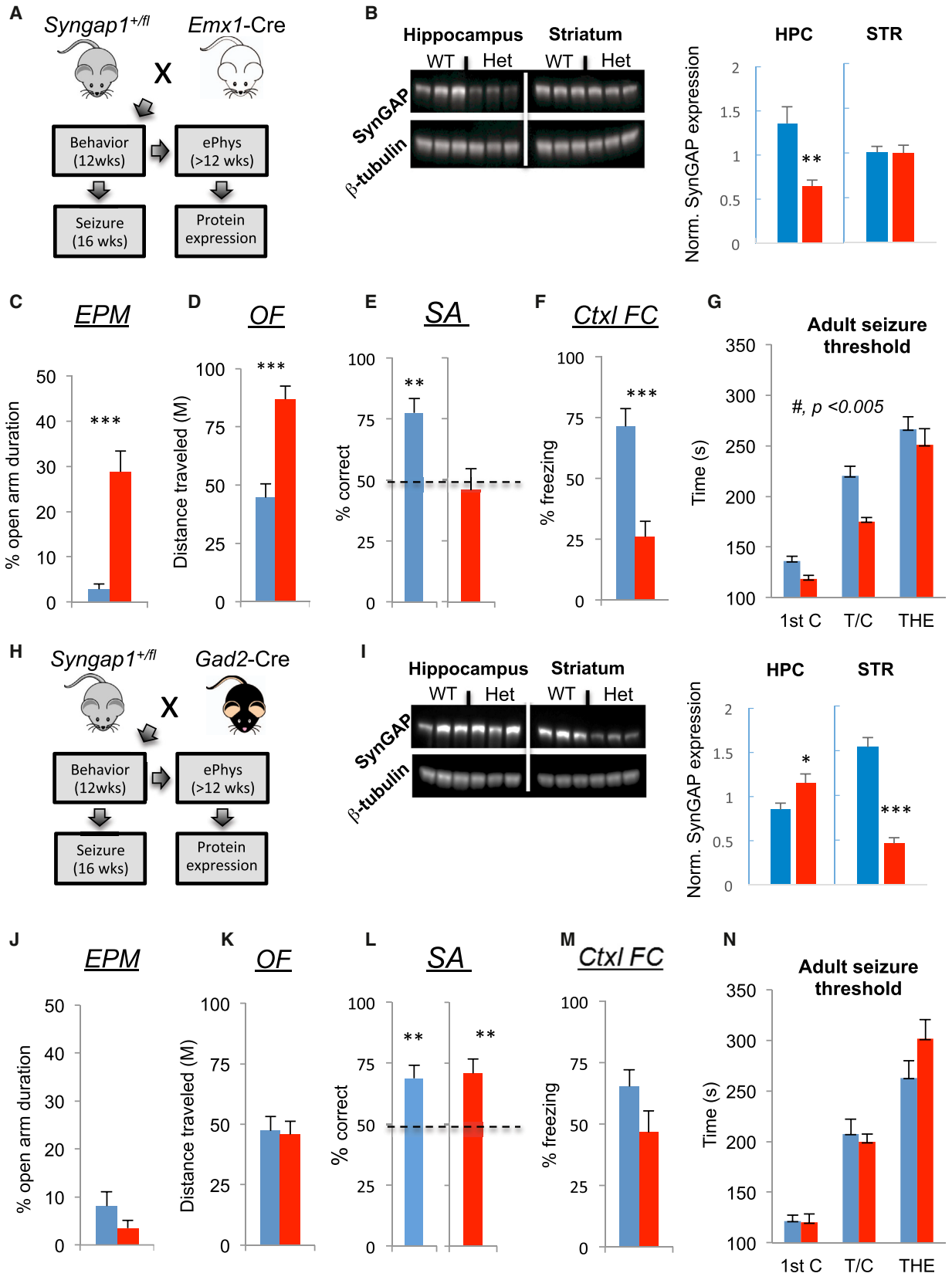

(legend on next page)

consistent with the idea that changes in adult L2/3 pyramidal neuron excitatory synaptic function is a secondary consequence of abnormal brain development. Based on our prior experiments demonstrating the predictive value of this adult physiological measure on cognitive ability, these data suggested that adult-induced haploinsufficiency would have negligible effects on cognition. Indeed, there was no change in core *Syngap1* behaviors; open field locomotion (Figure 7E), elevated plus maze open arm time (Figure 7F), the ability to spontaneous alternate in a T-maze (Figure 7G), and remote memory (Figure 7H). However, seizure threshold was reduced (Figures 7I and 7J), indicating that this behavior is dissociable from cognitive dysfunction and elevated cortical pyramidal cell excitatory synaptic function in *Syngap1* mutants.

Next, we explored the idea that stronger excitatory synaptic function in L2/3 pyramidal cells was unrelated to reduced SynGAP function in mature neurons, but instead is caused by a complex molecular process that originates within developing superficial pyramidal neurons. To test this, we exploited the ability to reverse pathogenic *Syngap1* mutations globally in the CNS (Clement et al., 2012). As a proof of principle, however, we first sought to discover a neurophysiological disruption in adult *Syngap1* mice that was sensitive to adult genetic reversal to demonstrate the effectiveness of this mouse model as a tool to differentiate developmental verses homeostatic consequences of pathogenic *Syngap1* mutations in brain cells. We chose to focus on long-term potentiation (LTP) deficits because they are well described in *Syngap1* Hets (Kim et al., 2003; Komiyama et al., 2002). Axonal excitability, release, and postsynaptic responses were not affected by *Syngap1* haploinsufficiency (Figures 8A–8C), although stabilization of LTP was drastically impaired in adult mutants (Figure 8D). Strikingly, LTP deficits were completely rescued by adult reversal of the pathogenic mutation (Figure 8D). We next conducted fluorescence deconvolution tomography (Chen et al., 2007; Vogel-Ciernia et al., 2013) to gain molecular insight into how pathogenic *Syngap1* mutations could disrupt the synaptic signaling steps thought to be involved in LTP consolidation (Rex et al., 2009). Slices were collected 2 minutes after LTP-inducing theta bursts and immunostained for PSD95 and Ras-GTP or phosphorylated ERK1/2 (Figure 8E). Theta bursts doubled the number of Ras-GTP+ excitatory synapses associated with high levels of Ras-GTP ($p = 0.012$, t test, two-tails) in WT, but not mutants ($p > 0.10$; Figure 8F, left). A similar pattern was found for p-ERK1/2; theta stimulation caused a pronounced increase in the double-labeled contacts in WT slices ($p < 0.0001$), but had no detectable effect in Hets ($p > 0.95$). Note that baseline levels of PSDs associated with high concentrations of p-ERK were substantially and significantly elevated relative to WTs in the mutants ($p = 0.029$, U-test; Figure 8F, right), indicating that reduced SynGAP protein in mature spines derepresses resting levels of activated ERK1/2. In accordance with the LTP results, conditional rescue of *Syngap1* haploinsufficiency returned the pERK1/2 response to theta bursts to levels obtained in WT mice (control versus theta bursts: $p = 0.002$). We further investigated group differences by counting the number of double-labeled synapses at various intensities of pERK1/2 immunostaining, an analysis that included all pERK-positive contacts. Theta bursts shifted the frequency distribution to the right in WT mice ($p < 0.0001$, two-way ANOVA; Figure 8G), as expected if the LTP-inducing stimulation increased the pool of activated kinase at a relatively small subset of synapses. A similar effect was observed for slices prepared from conditional rescue mice ($p < 0.0001$; Figure 8H), but was altogether absent ($p > 0.95$) in Hets (Figure 8I).

Figure 4. *Syngap1* Haploinsufficiency in Glutamatergic, but Not GABAergic, Neurons Mimics the Germline Mutant Endophenotype

(A) Experimental schematic depicts mouse breeding strategy and implementation timing of a behavioral test battery and flurothyl-induced seizures for adult offspring of an *Emx1*-Cre x Syngap1$^{+/fl}$ cross.

(B) Hippocampal (HPC) and dorsal striatal (STR) tissue were dissected from *Emx1*-Cre: Syngap1$^{+/+}$ and *Emx1*-Cre: Syngap1$^{+/fl}$ mice and processed for western blot analysis of SynGAP protein levels normalized to β-tubulin after behavioral and seizure paradigm testing. Normalized density - unpaired t test: n = 6 WT, n = 6 mutant, HPC: t(10) = 3.45; p = 0.0063; STR: t(10) = 0.051; p = 0.96.

(C–F) *Emx1*-Cre;Syngap1$^{+/+}$ and *Emx1*-Cre;Syngap1$^{+/fl}$ mice were run in a behavioral battery consisting of an elevated plus maze task (EPM), an open field test (OFT), an unforced discrete-two-trial spontaneous alternation task (SA), and a contextual fear conditioning paradigm. Unpaired t tests were performed for EPM, OF, and Ctxl FC tests. One-sample t test with 50% chance level as hypothetical mean were performed with each group for SA. EPM - % Open arm duration: n = 16 WT, n = 18 mutant, t(32) = 5.44, p = 5.48E-06. OF - distance traveled (M): n = 12 WT, n = 12, t(22) = 5.18; p = 3.39E-05. SA - % alternation: n = 10 WT, t(9) = 4.71; p = 0.0011; n = 12 mutant: t(11) = 0.48; p = 0.64. Ctxl FC - % freezing: n = 7 WT, n = 10 mutant, t(15) = 4.44, p = 0.00036.

(G) *Emx1*-Cre: Syngap1$^{+/+}$ and *Emx1*-Cre: Syngap1$^{+/fl}$ mice were subjected to a flurothyl-induced seizure paradigm. Time taken to reach three separate events, first clonus (1st C), tonic-clonic (T/C), and total hindlimb extension (THE), during the course of the procedure was measured and WT and HET groups compared within each of the two cohorts. RMANOVA - genotype effect: F(1,32) = 10.79; p = 0.0025; genotype x event interaction: F(2,64) = 1.67; p = 0.20.

(H) Experimental schematic depicts mouse breeding strategy and implementation timing of a behavioral test battery and flurothyl-induced seizures for adult offspring of a *Gad2*-Cre x Syngap1$^{+/fl}$ cross.

(I) Hippocampal (HPC) and dorsal striatal (STR) tissue were dissected from *Gad2*-Cre: Syngap1$^{+/+}$ and *Gad2*-Cre: Syngap1$^{+/fl}$ mice and processed for western blot analysis of SynGAP protein levels normalized to β-tubulin after behavioral and seizure paradigm testing. Normalized density - unpaired t test: n = 6 WT, n = 6 mutant, HPC: t(10) = 2.35; p = 0.040; STR: t(10) = 8.61; p = 0.00000612.

(J–M) *Gad2*-Cre: Syngap1$^{+/+}$ and *Gad2*-Cre: Syngap1$^{+/fl}$ mice were run in a behavioral battery consisting of an elevated plus maze task (EPM), an open field test (OFT), an unforced discrete-two-trial spontaneous alternation task (SA), and a contextual fear conditioning paradigm. Unpaired t tests were performed for EPM, OF, and Ctxl FC tests. One-sample t test with 50% chance level as hypothetical mean were performed with each group for SA. EPM - % Open arm duration: n = 16 WT, n = 14 mutant, t(28) = 1.30, p = 0.20. OF - distance traveled (M): n = 12 WT, n = 12, t(22) = 0.20; p = 0.85. SA - % alternation: n = 12 WT, t(11) = 3.45; p = 0.0055; n = 12 mutant, t(11) = 3.46; p = 0.0054. Ctxl FC - % freezing: n = 12 WT, n = 11 mutant, t(21) = 1.71, p = 0.1027.

(N) *Gad2*-Cre: Syngap1$^{+/+}$ and *Gad2*-Cre: Syngap1$^{+/fl}$ mice were subjected to a flurothyl-induced seizure paradigm. Time taken to reach three separate events, first clonus (1st C), tonic-clonic (T/C), and total hindlimb extension (THE), during the course of the procedure was measured and the two groups compared. RMANOVA - genotype effect-F(1,22) = 0.60; p = 0.45; genotype x event interaction-F(2,44) = 2.42; p = 0.10.

WT, blue; mutants, red for all bar graphs. Error bars represent SEM. *p < 0.05, **p < 0.01, ***p < 0.001.

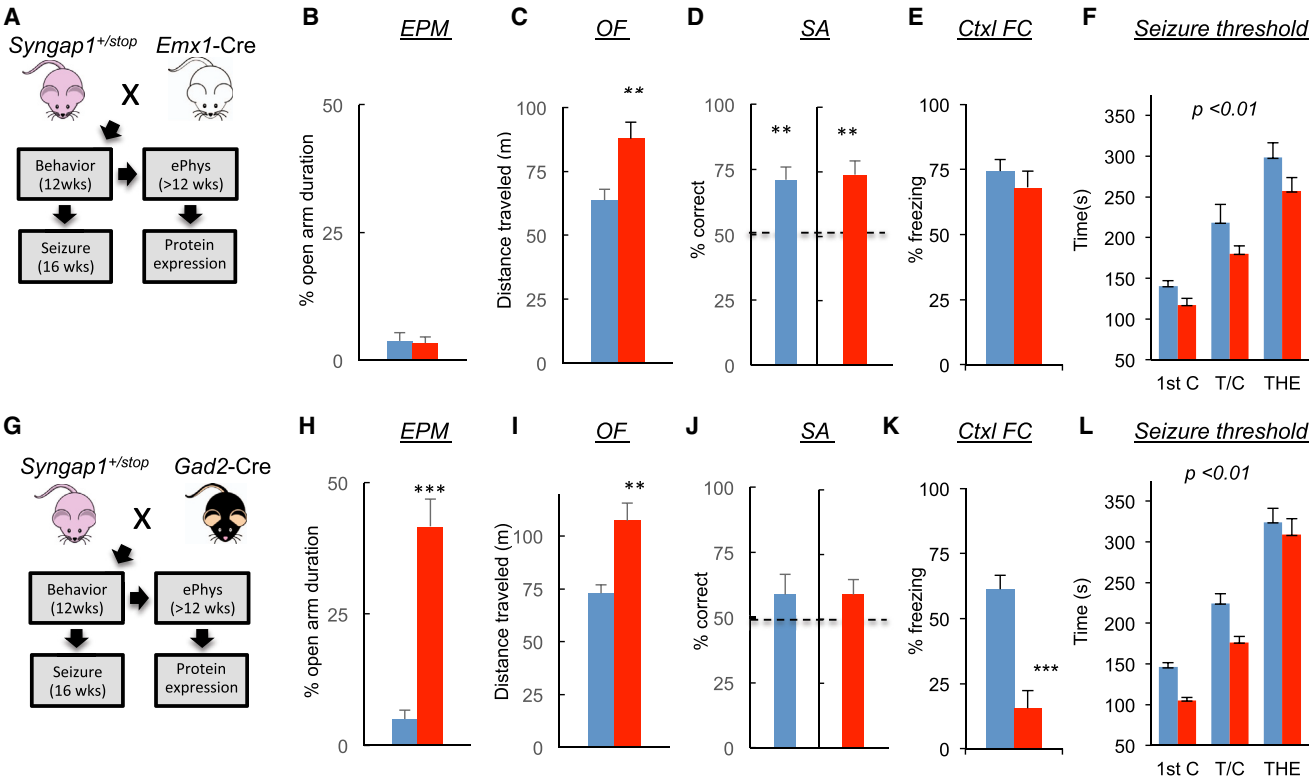

Figure 5. Reversal of Pathogenic Mutations in Forebrain Glutamatergic Neurons Is Sufficient to Rescue Cognitive and Emotional Endophenotypes Present in *Syngap1* Mutants

(A) Experimental schematic depicts mouse breeding strategy and implementation timing of a behavioral test battery and flurothyl-induced seizures for adult offspring of an *Emx1*-Cre x *Syngap1*$^{+/lx\text{-}st}$ cross.

(B–E) *Emx1*-Cre: Syngap1$^{+/+}$ and *Emx1*- *Syngap1*$^{+/lx\text{-}st}$ mice were run in a behavioral battery consisting of an elevated plus maze task (EPM), an open field test (OFT), an unforced discrete two-trial spontaneous alternation task (SA), and a contextual fear conditioning paradigm. Unpaired t tests were performed for EPM, OF, and Ctxl FC tests. One-sample t test with 50% chance level as hypothetical mean were performed with each group for SA. EPM - % Open arm duration: n = 15 WT, n = 15 mutant, t(28) = 0.21, p = 0.83. OF - distance traveled (M): n = 15 WT, n = 15, t(28) = 3.09; p = 0.0045. SA - % alternation: n = 15 WT, t(14) = 4.40; p = 0.00050; n = 15 mutant: t(14) = 4.43; p = 0.00060. Ctxl FC - % freezing: n = 11 WT, n = 11 mutant, t(20) = 0.81, p = 0.42.

(F) *Emx1*-Cre: Syngap1$^{+/+}$ and *Emx1*-Cre: *Syngap1*$^{+/lx\text{-}st}$ mice were subjected to a flurothyl-induced seizure paradigm. Time taken to reach three separate events, first clonus (1st C), tonic-clonic (T/C), and total hindlimb extension (THE), during the course of the procedure was measured and the two groups compared. RMANOVA - genotype effect: F(1,20) = 8.35; p = 0.0091; genotype x event interaction: F(2,40) = 0.22; p = 0.80.

(G) Experimental schematic depicts mouse breeding strategy and implementation timing of a behavioral test battery and flurothyl-induced seizures for adult offspring of a *Gad2*-Cre x *Syngap1*$^{+/lx\text{-}st}$ cross.

(H–K) *Gad2*-Cre: Syngap1$^{+/+}$ and *Gad2*-Cre: *Syngap1*$^{+/lx\text{-}st}$ mice were run in a behavioral battery consisting of an elevated plus maze task (EPM), an open field test (OFT), an unforced discrete two-trial spontaneous alternation task (SA), and a contextual fear conditioning paradigm. Unpaired t tests were performed for EPM, OF, and Ctxl FC tests. One-sample t test with 50% chance level as hypothetical mean was performed with each group for SA. EPM - % Open arm duration: n = 17 WT, n = 16 mutant, t(31) = 6.83, p = 9.92E-08. OF - distance traveled (M): n = 17 WT, n = 16, t(31) = 3.78; p = 0.00067. SA - % alternation: n = 17 WT, t(16) = 1.14; p = 0.27; n = 16 mutant, t(15) = 1.57; p = 0.14. Ctxl FC - % freezing: n = 13 WT, n = 12 mutant, t(23) = 5.36, p = 0.0000191.

(L) *Gad2*-Cre: Syngap1$^{+/+}$ and *Gad2*-Cre: *Syngap1*$^{+/lx\text{-}st}$ mice were subjected to a flurothyl-induced seizure paradigm. Time taken to reach three separate events, first clonus (1st C), tonic-clonic (T/C), and total hindlimb extension (THE), during the course of the procedure was measured and the two groups compared. RMANOVA - genotype effect-F(1,23) = 11.69; p = 0.0024; genotype x event interaction-F(2,46) = 0.96; p = 0.39.

WT, blue; mutants, red for all bar graphs. Error bars represent SEM. *p < 0.05, **p < 0.01, ***p < 0.001.

Finally, we measured mEPSCs from mPFC L2/3 pyramidal cells in WT, Het, and rescue animals to examine how SynGAP expression levels in adulthood influence this neurophysiological disruption that is also present in adult *Syngap1* mutants. In striking contrast to the hippocampal plasticity deficits, elevated synaptic strength in L2/3 Het pyramidal neurons was not improved by the adult genetic repair strategy (Figures 8J and 8K). Importantly, we confirmed that the frontal cortices of conventional *Syngap1* Hets also have elevated levels of p-ERK1/2 (Figure S6). Together, these findings support the idea that enhanced excitatory synaptic strength in superficial cortical pyramidal cells arises from developmental neuronal damage, indicating that this neurophysiological disruption is independent of homeostatic alterations to Ras/ERK dendritic spine signaling caused by low SynGAP levels in adult neurons. These data also further validate the predictive value of enhanced L2/3 excitatory synaptic strength in Het mice because adult reversal of pathogenic *Syngap1* mutations does not improve

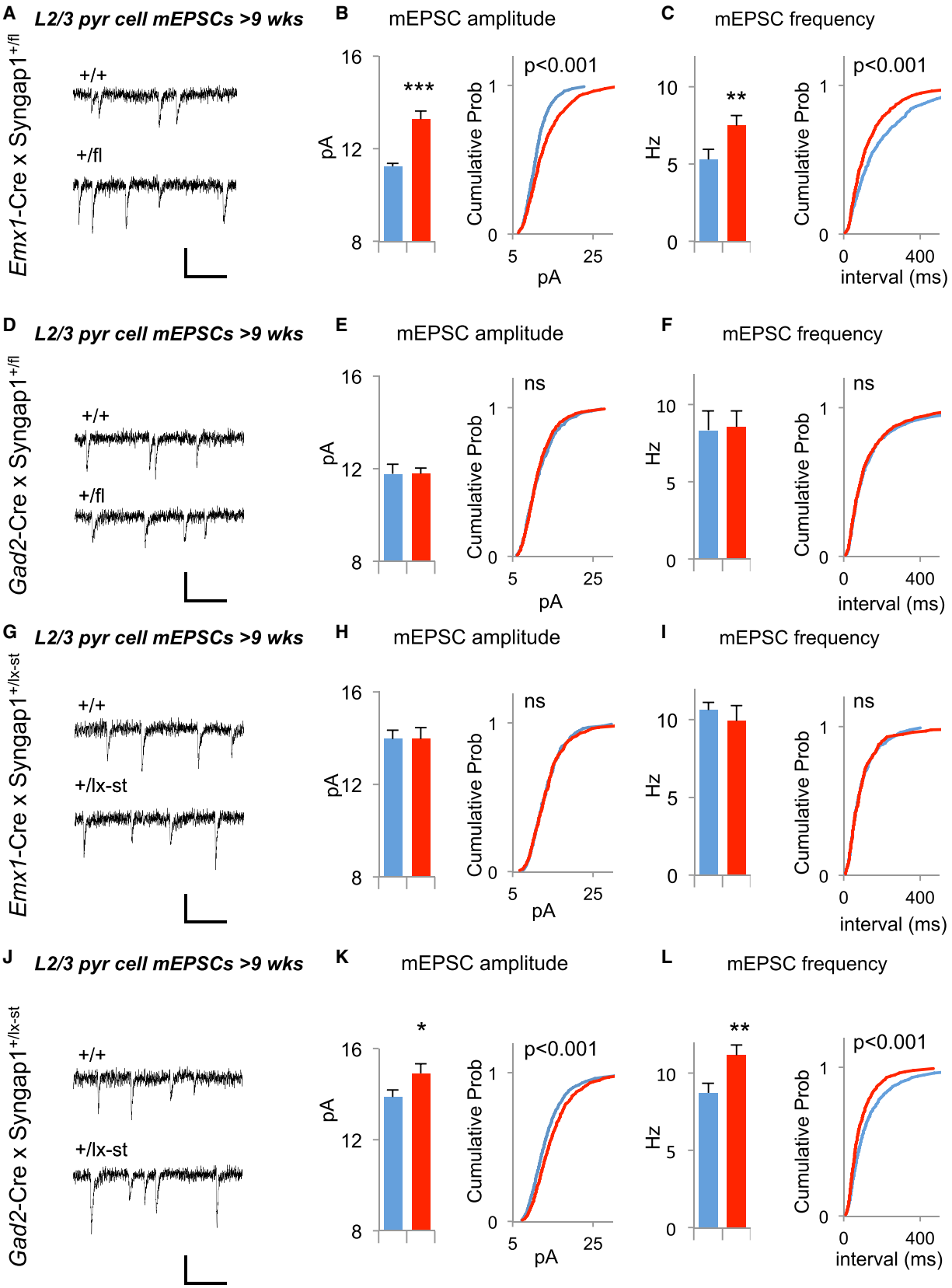

(legend on next page)

performance in behavioral measures of cognition (Clement et al., 2012).

DISCUSSION

There is a great interest in defining the brain regions and specific cell types responsible for cognitive deficits in NDDs, with the hope of developing tailor-made therapies for each specific condition. Prior studies in other models of NDDs suggest that cognition and behavioral adaptations are impaired through defects in a wide variety of cell types and circuits. However, not all cell types expressing the mutation are required to reproduce important elements of the disorder. For example, deletion of *MECP2* in GABAergic neurons phenotypically mimics the constitutive germline deletion (Chao et al., 2010), whereas restoration of gene function in glia provides significant rescue (Lioy et al., 2011). A similar relationship between GABAergic neuron dysfunction and NF1 mutations also exists (Cui et al., 2008). Interestingly, NF1, like *Syngap1*, is a RasGAP, although there is a clear distinction between the cell and temporal-specificity mediated by disruption to these two ID-related genes (see the Supplemental Experimental Procedures for a detailed comparison of these two RasGAP-related ID models). Cell type and brain region specificity has also been extensively studied in the Tsc1 model, where cerebellar neurons, astrocytes, and thalamic excitatory neurons have been implicated in various behavioral phenotypes (Meikle et al., 2007; Normand et al., 2013; Tsai et al., 2012; Uhlmann et al., 2002). Although cortical hyperexcitability results from excitatory neurons in Fmr1 knockout mice, cell type specificity of cognitive defects has not been thoroughly examined (Hays et al., 2011). Due to the robust nature of cognitive deficits in *Syngap1*$^{+/-}$ mice, we succeeded in identifying a sensitive cell type (e.g., forebrain pyramidal neurons) that is both necessary and sufficient to account for the bulk of the behavioral endophenotype. This specificity is highlighted by the minimal functional impact of these mutations in other cell types, such as GABAergic neurons located throughout the CNS. In addition to all forebrain pyramidal neurons, the EMX1 driver line used in this study causes Cre-mediated recombination in glial and Cajal-Retzius cells (Gorski et al., 2002). *Syngap1* is highly enriched in neurons (Kim et al., 1998). Thus, glia are unlikely to underlie major aspects of the mouse endophenotype. However, our results cannot rule out the possibility that other cell types, such as Cajal-Retzius cells, contribute to cognitive defects in *Syngap1* Hets.

Enhanced excitatory synaptic drive onto mature superficial pyramidal neurons resulting from the developmental impact of pathogenic *Syngap1* mutations may disrupt the computational power of local synaptic networks by affecting the coding of information (Petersen and Crochet, 2013). This idea is supported by the current findings of abnormal cortical discharges in mature *Syngap1* mutants. Interestingly, similar cortical discharges are observed in patients with human *Syngap1* haploinsufficiency (Berryer et al., 2013) and the presence of these types of high-frequency oscillations in humans is associated with reduced cognition (Nicolai et al., 2012). As a result, even if cellular and/or network signatures of hyperexcitability cannot be directly linked to reduced cognition in mature *Syngap1*$^{+/-}$ mice, the presence of similar measures of abnormal EEG signals in both mice and humans with pathogenic *Syngap1* mutations indicates the potential for them to serve as a robust endpoint in translational studies aimed at improving brain function and cognitive ability in patients.

Our current studies employing temporal and cell type-specific alterations of SynGAP expression further support the emerging idea that pathogenic *Syngap1* mutations cause cognitive abnormalities through developmental brain damage (Clement et al., 2012, 2013). Although we do not know the exact role of *Syngap1* during the developmental critical period, one possibility is that early synapse maturation caused by pathogenic disruptions to this gene (Clement et al., 2012, 2013) may permanently fix the adult spines to a larger size. Indeed, we have found that newly born spines in the developing

Figure 6. Enhanced L2/3 Excitatory Synaptic Function Is an Indicator of Reduced Cognition in *Syngap1* Mutants

(A) Example recordings of mEPSC events from +/+ and +/fl mice obtained by *Emx1*-Cre x Syngap1$^{+/fl}$ cross. Scale bar represents 20 pA, 100 ms.

(B) Bar graph and cumulative percentage plots show increased mEPSC amplitude in Emx1-Cre;+/fl mice (n = 10 +/+, n = 12 +/fl, t(20) = 4.92, p = 0.000082; two sample K-S test on cumulative percentage distribution Z = 4.24, p < 0.001).

(C) Bar graph and cumulative percentage plots show increased mEPSC frequency in Emx1-Cre;+/fl mice (n = 10 +/+, n = 12 +/fl, t(20) = 2.26, p = 0.035; two sample K-S test on cumulative percentage distribution Z = 3.39, p < 0.001).

(D) Example recordings of mEPSC events from +/+ and +/fl mice obtained by *Gad2*-Cre x Syngap1$^{+/fl}$ cross. Scale bar represents 20 pA, 100 ms.

(E) Bar graph and cumulative percentage plots show normal mEPSC amplitude in Gad2-Cre;+/fl mice (n = 11 +/+, n = 11 +/fl, t(20) = 0.03, p = 0.98; two sample K-S test on cumulative percentage distribution Z = 1.12, p = 0.16).

(F) Bar graph and cumulative percentage plots show normal mEPSC frequency in in Gad2-Cre;+/fl mice (n = 11 +/+, n = 11 +/fl, t(20) = 0.14, p = 0.89; two sample K-S test on cumulative percentage distribution Z = 0.69, p = 0.73).

(G) Example recordings of mEPSC events from +/+ and +/lx-st mice obtained by *Emx1*-Cre x Syngap1$^{+/lx\text{-}st}$ cross. Scale bar represents 20 pA, 100 ms.

(H) Bar graph and cumulative percentage plots show normal mEPSC amplitude in Emx1-Cre;+/lx-st mice (n = 17 +/+, n = 13 +/lx-st, t(28) = 0.00045, p = 0.99; two sample K-S test on cumulative percentage distribution Z = 0.62, p = 0.83).

(I) Bar graph and cumulative percentage plots show normal mEPSC frequency in in Emx1-Cre;+/lx-st mice (n = 17 +/+, n = 13 +/lx-st, t(28) = 0.68, p = 0.50; two sample K-S test on cumulative percentage distribution Z = 0.50, p = 0.96).

(J) Example recordings of mEPSC events from +/+ and +/lx-st mice obtained by *Gad2*-Cre x Syngap1$^{+/lx\text{-}st}$ cross. Scale bar represents 20 pA, 100 ms.

(K) Bar graph and cumulative percentage plots show increased mEPSC amplitude in Gad2-Cre;+/lx-st mice (n = 19 +/+, n = 19 +/lx-st, t(36) = 2.49, p = 0.017; two sample K-S test on cumulative percentage distribution Z = 3.86, p < 0.001).

(L) Bar graph and cumulative percentage plots show increased mEPSC frequency in Gad2-Cre;+/lx-st mice (n = 19 +/+, n = 19 +/lx-st, t(36) = 3.15, p = 0.0033. Two sample K-S test on cumulative percentage distribution Z = 4.34, p < 0.001).

WT, blue; mutants, red for all bar graphs. Error bars represents SEM. *p < 0.05, **p < 0.01, ***p < 0.001.

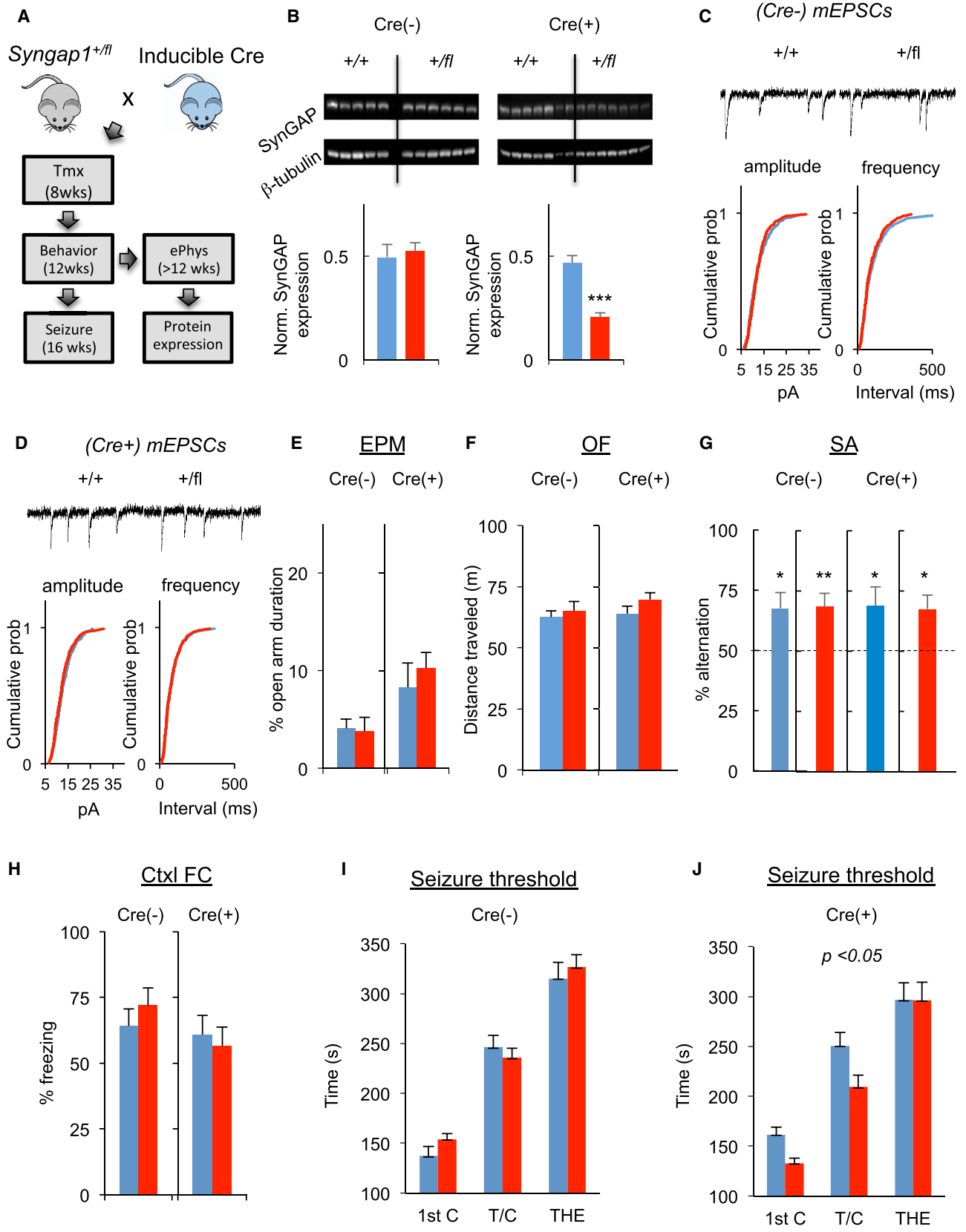

(legend on next page)

Syngap1 mutant brain are larger than nascent spines born to WT neurons (M. Aceti and G.R., unpublished data). Dendritic spine volume is tightly coupled to AMPA receptor function at individual postsynapses in both the cortex and hippocampus (Matsuzaki et al., 2001; Noguchi et al., 2011). Thus, abnormally large spines in mature cortical pyramidal cells in *Syngap1* mice may degrade the ability of these neurons to scale down synaptic excitation in response to environmental stimuli or changing social conditions (Wang et al., 2011). Indeed, according to the principle of homeostatic regulation of neuronal firing rates (Turrigiano, 2008), excitatory synapses in *Syngap1* mutants would be expected to scale down their strengths to compensate for the enhanced network excitability that is clearly present in these mice. Thus, the gradual emergence of elevated excitatory synaptic function in L2/3 neurons as a secondary consequence of *Syngap1* disruption in development is representative of an altered form of synaptic homeostasis that degrades the ability of mature L2/3 neurons to optimally balance excitation relative to inhibition.

EXPERIMENTAL PROCEDURES

The generation of conventional Syngap1+/− mice (Kim et al., 2003), conditional knockout line (Syngap1+/fl), and conditional rescue line (Syngap1+/lx-st) has been described previously (Clement et al., 2012). All Syngap1 mice are maintained on a BL6/B129sv/ev hybrid background as previously described (Clement et al., 2012; Guo et al., 2009). Emx1-Cre (#05628), Gad2-Cre (#10802), PV-Cre (#8069), Inducible CAG-Cre-ERt (#004682), TdTomato Ai9 (#007905), and GIN-GFP (#03718) lines were purchased from Jackson Laboratories. According to the supplier, these lines are maintained on a pure C57/BL6j background (n > 5 generations), except for the PV-Cre line, which is on a hybrid B6;129p2 background, and the GIN-GFP line, which is on a FVB/NJ background. In general, male Cre drivers were used in mating schemes, except for EMX1-ires-Cre crosses, due to rare occurrences of Cre activity in sperm cells. Video EEG recordings lasted for 2 weeks and random samples of the recordings were analyzed for evidence of spiking. VSD imaging in cortical slices was performed as previously described (Clement et al., 2012; Xu et al., 2010). mPFC slices for whole cell electrophysiology experiments were prepared as described elsewhere (Clement et al., 2013). Behavioral paradigms, tamoxifen injections, and fluorothyl-induced seizure protocol were carried out as described previously (Clement et al., 2012). Extracellular slice physiology and fluorescence deconvolution tomography has been described in detail elsewhere (Babayan et al., 2012; Chen et al., 2007, 2010; Vogel-Ciernia et al., 2013). All proposed animal research was approved by the TSRI Animal Care and Use Committee and the studies were subsequently overseen by this office. For precise details pertaining to all experimental procedures used in this in this study, please refer to the Supplemental Experimental Procedures.

SUPPLEMENTAL INFORMATION

Supplemental Information includes Supplemental Experimental Procedures, six figures, and one table and can be found with this article online at http://dx.doi.org/10.1016/j.neuron.2014.05.015.

AUTHOR CONTRIBUTIONS

E.D.O., T.K.C., E.A.K., C.R., R.R.S., A.H.B., Y.S., and R.L. performed research. E.D.O., T.K.C., X.X., J.L.N., C.A.M., G.L., and G.R. designed experiments. E.D.O., T.K.C., E.A.K., C.R., R.R.S., A.H.B., Y.S., R.L., X.X., J.L.N,. C.A.M., G.L., and G.R. analyzed data. E.D.O., T.K.C., and G.R. wrote the manuscript. E.D.O., T.K.C., X.X., J.L.N., C.A.M., G.L., and G.R. edited the manuscript. E.D.O. and G.R. conceived the study.

ACKNOWLEDGMENTS

G.R. was supported by The National Institute for Neurological Disorders and Stroke (R01NS064079) and The National Institute for Mental Health (R01MH096847). C.A.M. was supported by grants from the National Institute for Drug Abuse (R01 DA034116; R03 DA033499). G.R. and C.A.M. were both supported by the Scripps Florida Fund. J.L.N. was supported by The National Institute for Neurological Disorders and Stroke grant NS29709. G.L. was supported by The National Institute for Neurological Disorders and Stroke grants NS085709 and NS045260 and the UCI Center for Autism Research and Treatment.

Figure 7. Global Induction of *Syngap1* Haploinsufficiency in Adulthood Has a Minimal Impact on L2/3 Synaptic Function and Behavior

(A) Experimental strategy to induce *Syngap1* haploinsufficiency during adulthood. Following a cross between *Syngap1*$^{+/fl}$ and hemizygous CreERt transgenic mice, the following four groups of mice were generated and used for experiments: Cre(−)/*Syngap1*$^{+/+}$, Cre(−)/*Syngap1*$^{+/fl}$, Cre(+)/*Syngap1*$^{+/+}$, and Cre(+)/*Syngap1*$^{+/fl}$. All animals were injected with tamoxifen at 8 weeks of age.

(B) Hippocampal (HPC) tissue was dissected from Cre(−)/*Syngap1*$^{+/+}$, Cre(−) /*Syngap1*$^{+/fl}$, Cre(+)/*Syngap1*$^{+/+}$, and Cre(+)/*Syngap1*$^{+/fl}$ mice and processed for western blot analysis of SynGAP protein levels normalized to β-tubulin after behavioral and seizure paradigm testing. Normalized density - unpaired t test - Cre(−): n = 5 WT, n = 6 mutant, t(9) = 0.44; p = 0.66; Cre(+): n = 7 WT, n = 7 mutant, t(12) = 6.86; p = 0.00000174.

(C) Cumulative percentage plots and example recordings show normal mEPSC amplitude and frequency in (Cre−) animals. (n = 11 +/+, n = 11 +/fl; mean mEPSC amplitudes 12.59 ± 0.48 +/+, 12.83 ± 0.35 +/fl, t(20) = 0.40, p = 0.69; mean mEPSC frequencies 10.14 ± 1.07 +/+, 11.25 ± 0.65 +/fl, t(20) = 0.89, p = 0.38; two sample K-S test on cumulative percentage distributions: Z = 1.07, p = 0.2 for mEPSC amplitude; Z = 1.02, p = 0.25 for mEPSC interevent interval).

(D) Cumulative percentage plots and example recordings show normal mEPSC amplitude and frequency in (Cre+) animals. (n = 12 +/+, n = 12 +/fl; mean mEPSC amplitudes 13.04 ± 0.24 +/+, 12.67 ± 0.47 +/fl; mean mEPSC frequencies 12.33 ± 0.67 +/+, 12.08 ± 0.74 +/fl, t(22) = 0.70, p = 0.49; t(22) = 0.25, p = 0.80; two sample K-S test on cumulative percentage distributions Z = 1.28, p = 0.07 for mEPSC amplitude; Z = 0.59, p = 0.88 for mEPSC interevent interval).

(E–H) Cre(−)/*Syngap1*$^{+/+}$, Cre(−)/*Syngap1*$^{+/fl}$, Cre(+)/*Syngap1*$^{+/+}$, Cre(+)/*Syngap1*$^{+/fl}$ mice were run in a behavioral battery consisting of an elevated plus maze task (EPM), an open field test (OFT), an unforced discrete two-trial spontaneous alternation task (SA), and a contextual fear conditioning paradigm. Unpaired t tests were performed for EPM, OF, and Ctxl FC tests. One-sample t test with 50% chance level as hypothetical mean were performed with each group for SA. EPM - % Open arm duration - Cre(−): n = 15 WT, n = 18 mutant, t(31) = 0.16, p = 0.87; Cre(+):n = 16 WT, n = 17 mutant, t(31) = 0.68, p = 0.50. OF - distance traveled (M) - Cre(−):n = 15 WT, n = 16 mutant, t(29) = 0.55, p = 0.59; Cre(+): n = 16 WT, n = 17 mutant, t(31) = 1.40, p = 0.17. SA - % alternation - Cre(−)/*Syngap1*$^{+/+}$: t(12) = 2.63, p = 0.022; Cre(−)/*Syngap1*$^{+/fl}$: t(14) = 3.21, p = 0.0062; Cre(+)/*Syngap1*$^{+/+}$: t(15) = 2.42, p = 0.028; Cre(+)/*Syngap1*$^{+/fl}$: t(12) = 2.92, p = 0.013. Ctxl FC - % freezing: Cre(−): n = 11 WT, n = 11 mutant, t(20) = 0.83, p = 0.41. Cre(+):n = 13 WT, n = 9 mutant, t(20) = 0.4, p = 0.69.

(I and J) Cre(−)/*Syngap1*$^{+/+}$, Cre(−)/*Syngap1*$^{+/fl}$, Cre(+)/*Syngap1*$^{+/+}$, Cre(+)/*Syngap1*$^{+/fl}$ mice were subjected to a flurothyl-induced seizure paradigm. Time taken to reach three separate events, first clonus (1st C), tonic-clonic (T/C), and total hindlimb extension (THE), during the course of the procedure were measured and WT and HET groups compared within each of the Cre(−) and Cre(+) groups. RMANOVA – Cre(−): genotype effect-F(1,25) = 0.22; p = 0.64; genotype x event interaction-F(2,50) = 0.66; p = 0.52. Cre(+): genotype effect-F(1,22) = 4.58; p = 0.044; genotype x event interaction-F(2,44) = 2.18; p = 0.12.

WT, blue; mutants, red for all bar graphs. Error bars represent SEM. *p < 0.05, **p < 0.01, ***p < 0.001.

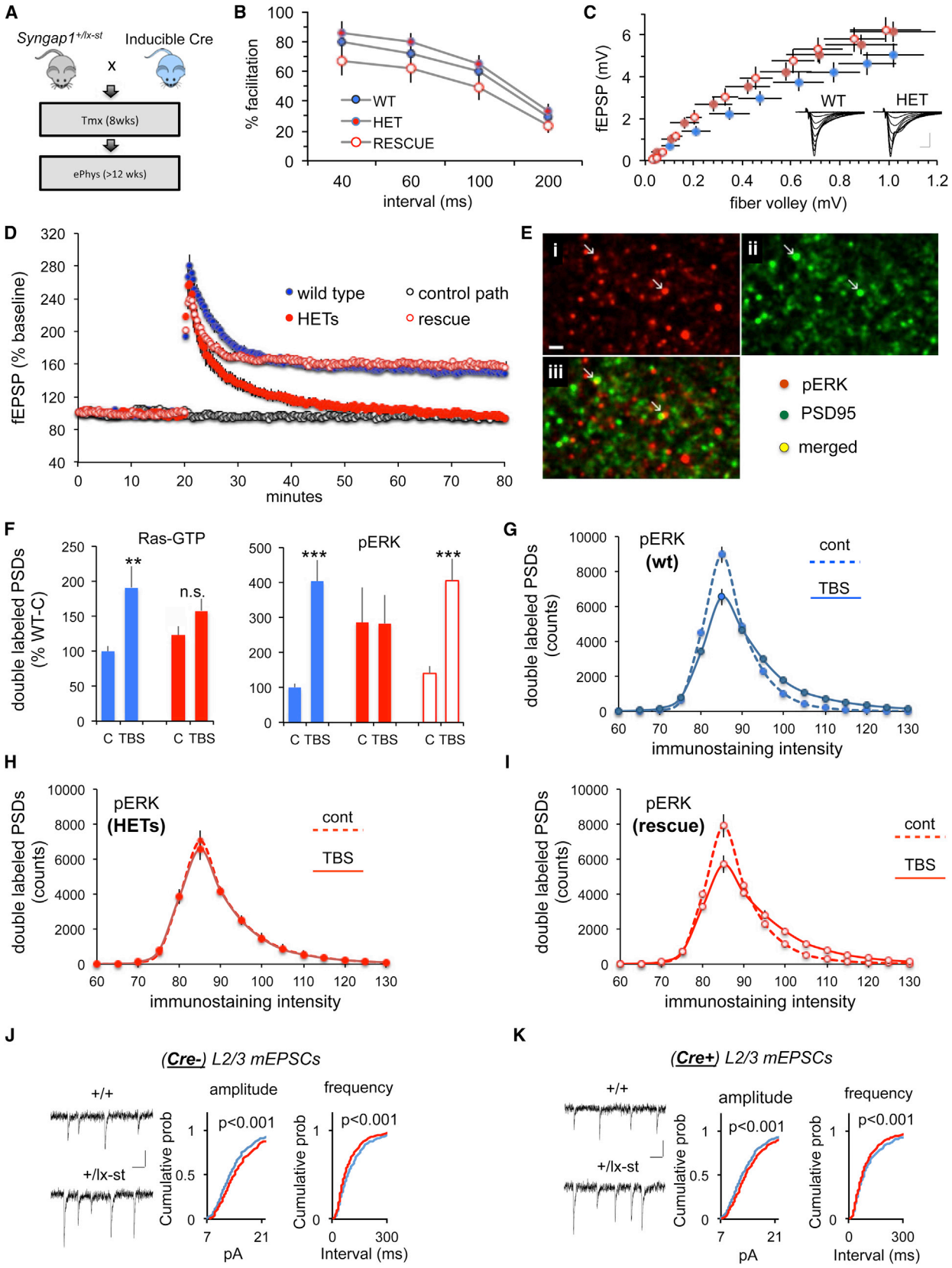

(legend on next page)

Accepted: April 24, 2014
Published: June 18, 2014

REFERENCES

Babayan, A.H., Kramar, E.A., Barrett, R.M., Jafari, M., Haettig, J., Chen, L.Y., Rex, C.S., Lauterborn, J.C., Wood, M.A., Gall, C.M., and Lynch, G. (2012). Integrin dynamics produce a delayed stage of long-term potentiation and memory consolidation. J. Neurosci. *32*, 12854–12861.

Berryer, M.H., Hamdan, F.F., Klitten, L.L., Møller, R.S., Carmant, L., Schwartzentruber, J., Patry, L., Dobrzeniecka, S., Rochefort, D., Neugnot-Cerioli, M., et al. (2013). Mutations in SYNGAP1 cause intellectual disability, autism, and a specific form of epilepsy by inducing haploinsufficiency. Hum. Mutat. *34*, 385–394.

Carvill, G.L., Heavin, S.B., Yendle, S.C., McMahon, J.M., O'Roak, B.J., Cook, J., Khan, A., Dorschner, M.O., Weaver, M., Calvert, S., et al. (2013). Targeted resequencing in epileptic encephalopathies identifies de novo mutations in CHD2 and SYNGAP1. Nat. Genet. *45*, 825–830.

Centers for Disease Control and Prevention (CDC) (2004). Economic costs associated with mental retardation, cerebral palsy, hearing loss, and vision impairment—United States, 2003. MMWR Morb. Mortal. wkly. Rep. *53*, 57–59.

Chao, H.T., Chen, H., Samaco, R.C., Xue, M., Chahrour, M., Yoo, J., Neul, J.L., Gong, S., Lu, H.C., Heintz, N., et al. (2010). Dysfunction in GABA signalling mediates autism-like stereotypies and Rett syndrome phenotypes. Nature *468*, 263–269.

Chen, H.J., Rojas-Soto, M., Oguni, A., and Kennedy, M.B. (1998). A synaptic Ras-GTPase activating protein (p135 SynGAP) inhibited by CaM kinase II. Neuron *20*, 895–904.

Chen, L.Y., Rex, C.S., Casale, M.S., Gall, C.M., and Lynch, G. (2007). Changes in synaptic morphology accompany actin signaling during LTP. J. Neurosci. *27*, 5363–5372.

Chen, L.Y., Rex, C.S., Babayan, A.H., Kramár, E.A., Lynch, G., Gall, C.M., and Lauterborn, J.C. (2010). Physiological activation of synaptic Rac>PAK (p-21 activated kinase) signaling is defective in a mouse model of fragile X syndrome. J. Neurosci. *30*, 10977–10984.

Clement, J.P., Aceti, M., Creson, T.K., Ozkan, E.D., Shi, Y., Reish, N.J., Almonte, A.G., Miller, B.H., Wiltgen, B.J., Miller, C.A., et al. (2012). Pathogenic SYNGAP1 mutations impair cognitive development by disrupting maturation of dendritic spine synapses. Cell *151*, 709–723.

Clement, J.P., Ozkan, E.D., Aceti, M., Miller, C.A., and Rumbaugh, G. (2013). SYNGAP1 links the maturation rate of excitatory synapses to the duration of critical-period synaptic plasticity. J. Neurosci. *33*, 10447–10452.

Cui, Y., Costa, R.M., Murphy, G.G., Elgersma, Y., Zhu, Y., Gutmann, D.H., Parada, L.F., Mody, I., and Silva, A.J. (2008). Neurofibromin regulation of ERK signaling modulates GABA release and learning. Cell *135*, 549–560.

de Ligt, J., Willemsen, M.H., van Bon, B.W., Kleefstra, T., Yntema, H.G., Kroes, T., Vulto-van Silfhout, A.T., Koolen, D.A., de Vries, P., Gilissen, C., et al. (2012). Diagnostic exome sequencing in persons with severe intellectual disability. N. Engl. J. Med. *367*, 1921–1929.

Doran, C.M., Einfeld, S.L., Madden, R.H., Otim, M., Horstead, S.K., Ellis, L.A., and Emerson, E. (2012). How much does intellectual disability really cost? First estimates for Australia. J. Intellect. Dev. Disabil. *37*, 42–49.

Gorski, J.A., Talley, T., Qiu, M., Puelles, L., Rubenstein, J.L., and Jones, K.R. (2002). Cortical excitatory neurons and glia, but not GABAergic neurons, are produced in the Emx1-expressing lineage. J. Neurosci. *22*, 6309–6314.

Guo, X., Hamilton, P.J., Reish, N.J., Sweatt, J.D., Miller, C.A., and Rumbaugh, G. (2009). Reduced expression of the NMDA receptor-interacting protein SynGAP causes behavioral abnormalities that model symptoms of Schizophrenia. Neuropsychopharmacology *34*, 1659–1672.

Hamdan, F.F., Gauthier, J., Spiegelman, D., Noreau, A., Yang, Y., Pellerin, S., Dobrzeniecka, S., Côté, M., Perreau-Linck, E., Carmant, L., et al.; Synapse to Disease Group (2009). Mutations in SYNGAP1 in autosomal nonsyndromic mental retardation. N. Engl. J. Med. *360*, 599–605.

Hamdan, F.F., Daoud, H., Piton, A., Gauthier, J., Dobrzeniecka, S., Krebs, M.O., Joober, R., Lacaille, J.C., Nadeau, A., Milunsky, J.M., et al. (2011a). De novo SYNGAP1 mutations in nonsyndromic intellectual disability and autism. Biol. Psychiatry *69*, 898–901.

Hamdan, F.F., Gauthier, J., Araki, Y., Lin, D.T., Yoshizawa, Y., Higashi, K., Park, A.R., Spiegelman, D., Dobrzeniecka, S., Piton, A., et al.; S2D Group

Figure 8. Global Rescue of Pathogenic *Syngap1* Mutations in Adulthood Has a Differential Effect on Synaptic Defects Originating in Distinct Types of EMX1+ Neurons

(A) Experimental strategy to induce *Syngap1* haploinsufficiency during adulthood. Following a cross between *Syngap1*$^{+/fl}$ and hemizygous CreERt transgenic mice, the following four groups of mice were generated and used for experiments: Cre(−)/*Syngap1*$^{+/+}$, Cre(−)/*Syngap1*$^{+/fl}$, Cre(+)/*Syngap1*$^{+/+}$, Cre(+)/*Syngap1*$^{+/fl}$. All animals were injected with tamoxifen at 8 weeks of age.

(B) Paired pulse facilitation curves (initial slope of fEPSP versus intervals between two stimulation pulses) for the indicated three groups of hippocampal slices. There were no statistically meaningful differences.

(C) Input/output curves (response size versus magnitude of fiber volley) for the three groups. Stimulation current was increased across a series of steps and the two variables measured. Inset: representative traces collected from WT and HET mice at each step in the input/output curve. Scale represents 1 mV/5 ms.

(D) Magnitude of LTP following delivery of a single train of five theta bursts. The slope of the fEPSP was normalized to the mean value for a 10-minute baseline period; shown are group means and SE. The control path, to the same site at which LTP was recorded, received 3/min pulses throughout the session.

(E) Dual immunostaining (PSD95 and p-ERK1/2) of a section through a hippocampal slice collected 2 min after a theta burst train. The images were processed using the fluorescence deconvolution tomography techniques described in the Experimental Procedures. Intensely labeled structures are shown. (i: p-ERK1/2; ii: PSD95; iii: merged images; also note arrows).

(F) Number of PSD95-positive puncta satisfying size and eccentricity constraints for synapses associated with very dense labeling for Ras-GTP (left) or pERK (right) from the zone surrounding a recording electrode in slices that received theta bursts (TBS) or low-frequency baseline stimulation only (C). Values are percentages of the double labeling counts for WT slices given control baseline stimulation. Asterisks represent statistical significance for the matched control versus TBS cases (two-tailed t tests for unequal variance. **p = 0.012; ***p = 0.002; ****p < 0.0001).

(G) Counts of synapses associated with the indicated intensities of pERK1/2 labeling for slices given control baseline stimulation (dashed line) or TBS (solid line) from WT slices; interaction term for two 2-way ANOVA comparing curves for control versus TBS groups ($F(31,928) = 14.54$; $p < 0.0001$).

(H) Same as (F) for control and TBS cases from rescue slices ($F(31,416) = 7.44$; $p < 0.0001$).

(I) Same as (F) for slices prepared from heterozygotes ($F(31,416) = 0.33$; $p > 0.95$).

(J) Cumulative percentage plots and example recordings show increased mEPSC amplitude and frequency in (Cre−) animals. (n = 17 +/+, n = 17 +/lx-st; mean mEPSC amplitudes 14.09 ± 0.30 +/+, 15.16 ± 0.41 +/lx-st, $t(32) = 2.08$, $p = 0.045$; mean mEPSC frequencies 8.89 ± 0.60 +/+, 11.11 ± 0.75 +/lx-st, $t(32) = 2.30$, $p = 0.028$; Two sample K-S test on cumulative percentage distributions: $Z = 2.89$, $p < 0.001$ for mEPSC amplitude; $Z = 3.22$, $p < 0.001$ for mEPSC interevent interval).

(K) Cumulative percentage plots and example recordings show increased mEPSC amplitude and frequency in (Cre+) animals. (n = 21 +/+, n = 16 +/lx-st; mean mEPSC amplitudes 13.79 ± 0.29 +/+, 14.79 ± 0.30 +/lx-st, $t(35) = 2.31$, $p = 0.027$; mean mEPSC frequencies 9.16 ± 0.66 +/+, 10.95 ± 0.75 +/lx-st, $t(35) = 2.03$, $p = 0.05$; Two sample K-S test on cumulative percentage distributions $Z = 2.92$, $p < 0.001$ for mEPSC amplitude; $Z = 2.80$, $p < 0.001$ for mEPSC interevent interval).

(2011b). Excess of de novo deleterious mutations in genes associated with glutamatergic systems in nonsyndromic intellectual disability. Am. J. Hum. Genet. *88*, 306–316.

Hays, S.A., Huber, K.M., and Gibson, J.R. (2011). Altered neocortical rhythmic activity states in Fmr1 KO mice are due to enhanced mGluR5 signaling and involve changes in excitatory circuitry. J. Neurosci. *31*, 14223–14234.

Helm, J., Akgul, G., and Wollmuth, L.P. (2013). Subgroups of parvalbumin-expressing interneurons in layers 2/3 of the visual cortex. J. Neurophysiol. *109*, 1600–1613.

Hippenmeyer, S., Vrieseling, E., Sigrist, M., Portmann, T., Laengle, C., Ladle, D.R., and Arber, S. (2005). A developmental switch in the response of DRG neurons to ETS transcription factor signaling. PLoS Biol. *3*, e159.

Kim, J.H., Liao, D., Lau, L.F., and Huganir, R.L. (1998). SynGAP: a synaptic RasGAP that associates with the PSD-95/SAP90 protein family. Neuron *20*, 683–691.

Kim, J.H., Lee, H.K., Takamiya, K., and Huganir, R.L. (2003). The role of synaptic GTPase-activating protein in neuronal development and synaptic plasticity. J. Neurosci. *23*, 1119–1124.

Komiyama, N.H., Watabe, A.M., Carlisle, H.J., Porter, K., Charlesworth, P., Monti, J., Strathdee, D.J., O'Carroll, C.M., Martin, S.J., Morris, R.G., et al. (2002). SynGAP regulates ERK/MAPK signaling, synaptic plasticity, and learning in the complex with postsynaptic density 95 and NMDA receptor. J. Neurosci. *22*, 9721–9732.

Kozlenkov, A., Roussos, P., Timashpolsky, A., Barbu, M., Rudchenko, S., Bibikova, M., Klotzle, B., Byne, W., Lyddon, R., Di Narzo, A.F., et al. (2014). Differences in DNA methylation between human neuronal and glial cells are concentrated in enhancers and non-CpG sites. Nucleic Acids Res. *42*, 109–127.

Krepischi, A.C., Rosenberg, C., Costa, S.S., Crolla, J.A., Huang, S., and Vianna-Morgante, A.M. (2010). A novel de novo microdeletion spanning the SYNGAP1 gene on the short arm of chromosome 6 associated with mental retardation. Am. J. Med. Genet. A. *152A*, 2376–2378.

Lazarus, M.S., and Huang, Z.J. (2011). Distinct maturation profiles of perisomatic and dendritic targeting GABAergic interneurons in the mouse primary visual cortex during the critical period of ocular dominance plasticity. J. Neurophysiol. *106*, 775–787.

Lioy, D.T., Garg, S.K., Monaghan, C.E., Raber, J., Foust, K.D., Kaspar, B.K., Hirrlinger, P.G., Kirchhoff, F., Bissonnette, J.M., Ballas, N., and Mandel, G. (2011). A role for glia in the progression of Rett's syndrome. Nature *475*, 497–500.

Madisen, L., Zwingman, T.A., Sunkin, S.M., Oh, S.W., Zariwala, H.A., Gu, H., Ng, L.L., Palmiter, R.D., Hawrylycz, M.J., Jones, A.R., et al. (2010). A robust and high-throughput Cre reporting and characterization system for the whole mouse brain. Nat. Neurosci. *13*, 133–140.

Matsuzaki, M., Ellis-Davies, G.C., Nemoto, T., Miyashita, Y., Iino, M., and Kasai, H. (2001). Dendritic spine geometry is critical for AMPA receptor expression in hippocampal CA1 pyramidal neurons. Nat. Neurosci. *4*, 1086–1092.

Meikle, L., Talos, D.M., Onda, H., Pollizzi, K., Rotenberg, A., Sahin, M., Jensen, F.E., and Kwiatkowski, D.J. (2007). A mouse model of tuberous sclerosis: neuronal loss of Tsc1 causes dysplastic and ectopic neurons, reduced myelination, seizure activity, and limited survival. J. Neurosci. *27*, 5546–5558.

Moon, I.S., Sakagami, H., Nakayama, J., and Suzuki, T. (2008). Differential distribution of synGAP alpha1 and synGAP beta isoforms in rat neurons. Brain Res. *1241*, 62–75.

Muhia, M., Yee, B.K., Feldon, J., Markopoulos, F., and Knuesel, I. (2010). Disruption of hippocampus-regulated behavioural and cognitive processes by heterozygous constitutive deletion of SynGAP. Eur. J. Neurosci. *31*, 529–543.

Nicolai, J., Ebus, S., Biemans, D.P., Arends, J., Hendriksen, J., Vles, J.S., and Aldenkamp, A.P. (2012). The cognitive effects of interictal epileptiform EEG discharges and short nonconvulsive epileptic seizures. Epilepsia *53*, 1051–1059.

Noguchi, J., Nagaoka, A., Watanabe, S., Ellis-Davies, G.C., Kitamura, K., Kano, M., Matsuzaki, M., and Kasai, H. (2011). In vivo two-photon uncaging of glutamate revealing the structure-function relationships of dendritic spines in the neocortex of adult mice. J. Physiol. *589*, 2447–2457.

Normand, E.A., Crandall, S.R., Thorn, C.A., Murphy, E.M., Voelcker, B., Browning, C., Machan, J.T., Moore, C.I., Connors, B.W., and Zervas, M. (2013). Temporal and mosaic Tsc1 deletion in the developing thalamus disrupts thalamocortical circuitry, neural function, and behavior. Neuron *78*, 895–909.

Petersen, C.C., and Crochet, S. (2013). Synaptic computation and sensory processing in neocortical layer 2/3. Neuron *78*, 28–48.

Porter, K., Komiyama, N.H., Vitalis, T., Kind, P.C., and Grant, S.G. (2005). Differential expression of two NMDA receptor interacting proteins, PSD-95 and SynGAP during mouse development. Eur. J. Neurosci. *21*, 351–362.

Rauch, A., Wieczorek, D., Graf, E., Wieland, T., Endele, S., Schwarzmayr, T., Albrecht, B., Bartholdi, D., Beygo, J., Di Donato, N., et al. (2012). Range of genetic mutations associated with severe non-syndromic sporadic intellectual disability: an exome sequencing study. Lancet *380*, 1674–1682.

Rex, C.S., Chen, L.Y., Sharma, A., Liu, J., Babayan, A.H., Gall, C.M., and Lynch, G. (2009). Different Rho GTPase-dependent signaling pathways initiate sequential steps in the consolidation of long-term potentiation. J. Cell Biol. *186*, 85–97.

Rumbaugh, G., Adams, J.P., Kim, J.H., and Huganir, R.L. (2006). SynGAP regulates synaptic strength and mitogen-activated protein kinases in cultured neurons. Proc. Natl. Acad. Sci. USA *103*, 4344–4351.

Taniguchi, H., He, M., Wu, P., Kim, S., Paik, R., Sugino, K., Kvitsiani, D., Fu, Y., Lu, J., Lin, Y., et al. (2011). A resource of Cre driver lines for genetic targeting of GABAergic neurons in cerebral cortex. Neuron *71*, 995–1013.

Tsai, P.T., Hull, C., Chu, Y., Greene-Colozzi, E., Sadowski, A.R., Leech, J.M., Steinberg, J., Crawley, J.N., Regehr, W.G., and Sahin, M. (2012). Autistic-like behaviour and cerebellar dysfunction in Purkinje cell Tsc1 mutant mice. Nature *488*, 647–651.

Turrigiano, G.G. (2008). The self-tuning neuron: synaptic scaling of excitatory synapses. Cell *135*, 422–435.

Uhlmann, E.J., Wong, M., Baldwin, R.L., Bajenaru, M.L., Onda, H., Kwiatkowski, D.J., Yamada, K., and Gutmann, D.H. (2002). Astrocyte-specific TSC1 conditional knockout mice exhibit abnormal neuronal organization and seizures. Ann. Neurol. *52*, 285–296.

Vogel-Ciernia, A., Matheos, D.P., Barrett, R.M., Kramár, E.A., Azzawi, S., Chen, Y., Magnan, C.N., Zeller, M., Sylvain, A., Haettig, J., et al. (2013). The neuron-specific chromatin regulatory subunit BAF53b is necessary for synaptic plasticity and memory. Nat. Neurosci. *16*, 552–561.

Wang, F., Zhu, J., Zhu, H., Zhang, Q., Lin, Z., and Hu, H. (2011). Bidirectional control of social hierarchy by synaptic efficacy in medial prefrontal cortex. Science *334*, 693–697.

Xu, X., Olivas, N.D., Levi, R., Ikrar, T., and Nenadic, Z. (2010). High precision and fast functional mapping of cortical circuitry through a novel combination of voltage sensitive dye imaging and laser scanning photostimulation. J. Neurophysiol. *103*, 2301–2312.

Zhang, W., Vazquez, L., Apperson, M., and Kennedy, M.B. (1999). Citron binds to PSD-95 at glutamatergic synapses on inhibitory neurons in the hippocampus. J. Neurosci. *19*, 96–108.